Water vapor stable isotope memory effects of common tubing materials

Alexandra L. Meyer[1], Lisa R. Welp[1]

[1]Department of Earth, Atmospheric, and Planetary Sciences, Purdue University, West Lafayette, 47907~~6~~, United States

Correspondence to: almeyer269@gmail.com or lwelp@purdue.edu

Abstract. Water molecules in vapor can exchange with water molecules sticking to surfaces of sampling tubing, and exchange rates are unique for each isotopologue and tubing material. Therefore, water molecules on tubing walls take some time to reach isotopic equilibrium with a new vapor isotopic signal. This creates a memory effect observed as attenuation time for signal propagation in continuous laser-based stable water vapor isotope measurement systems. ~~Therefore, isotopic equilibrium with a tubing walls creates a memory effect observed as attenuation time for signal propagation in continuous laser-based stable water vapor isotope measurement systems.~~ Tubing memory effects in δD and $\delta^{18}O$ measurements can limit the ability to observe fast changes, and because δD and $\delta^{18}O$ memory are not identical, this introduces transient deuterium excess (D-excess, defined as $\delta D - 8 * \delta^{18}O$) artifacts in time-varying observations. A comprehensive performance comparison of commonly used tubing material water exchange properties has not been published to our knowledge. We compared how a large isotopic step change propagated through five commonly used tubing materials, PFA, FEP, PTFE, HDPE, and copper, at two different temperatures and an air flow rate of 0.635~~1.1~~ L min^{-1} through approximately 100 feet (~30.5 m) of ~~1/4~~¼ ~~–~~ in.~~ch~~ (6.35 mm) outer diameter (OD) tubing. All tubing materials performed similarly to each other in terms of attenuation times, reaching 95 % completion in less than 45 seconds in all but 2 experiments ~~regardless of~~with slight variations based on temperature. ~~Bev-a-line~~Bev-A-Line XX was also tested, unheated, but it did not reach isotopic equilibrium after an hour, and we cannot recommend its use in water vapor applications. While shorter ~~inner diameter and length of~~ tubing length and smaller inner diameters shortens the delay of signal propagation through the tubing, they don't greatly change the shape of the attenuation curve or the delay-adjusted attenuation times under these conditions. ~~.This indicates that the speed of isotopic equilibrium of the tubing walls can be described as a first order chemical reaction controlled by the concentration of reactive surface sites rather than the total number of sites. Likewise, use of a high surface area particle filter at this air flow rate did not affect the speed of the isotopic signal attenuation. However, the addition of a mass flow meter did affect the speed of the attenuation, and we recommend investigating the influence of similar devices during measurement inlet and system design.~~ Our results show that these commonly-used plastic tubing materials are not inferior to copper in terms of isotopic memory under these conditions, and they are easier to work with and are less expensive than copper. Our experience and results from other published studies indicate that ~~Users are still advised to~~ maximi~~z~~zinge air flow rates ~~through both~~through the analyzer ~~and tubing~~ is the most effective way ~~and tubing~~ to minimize memory effects ~~especially~~ when accurate ~~time-varying~~high-frequency D-excess measurements are desired~~ required~~.

Formatted: Not Highlight

Formatted: Not Highlight

Formatted: Not Superscript/ Subscript

Formatted: Not Superscript/ Subscript

Formatted: Not Highlight

Formatted: Not Highlight

Formatted: Not Highlight

Formatted: Not Highlight

Formatted: Highlight

1 Introduction

In ~~–~~ situ laser absorption spectroscopy of water vapor isotopologues has risen in use over the last two decades~~ and a half~~ enabling fast, continuous isotopic measurements (Webster and Heymsfield, 2003; Lee et al., 2005; Griffith et al., 2006; Kerstel et al., 2006). All experimental setups inherently attenuate signal variability due to mixing in the analyzer optical cavities and molecular water interactions with surfaces inside the inlet and analyzer system, especially when different H_2O_v concentrations lead to wetting and drying of the tubing walls. The timescale for signal attenuation can vary greatly based on a wide range of tubing materials, air flow rates, temperatures, and pressures used (Sturm and Knohl, 2010; Griffis et al., 2010; Schmidt et al., 2010; Tremoy et al., 2011; Aemisegger

et al., 2012; Galewsky et al., 2016). As condensation in tubing is a concern due to liquid-vapor fractionation, many installations heat the tubing above ambient temperature, use a critical orifice at the tubing inlet to drop pressure in the lines, or do both in order to keep the vapor in the tubing above the dew point (e.g. Griffis et al. 2010; Luo et al. 2019).

Initially, a plastic coated aluminum Synflex tubing (also known as Dekabon or Dekoron) commonly used in the carbon dioxide and water eddy covariance flux community was used in water vapor isotope experiments (Lee et al., 2005; Gupta et al., 2009; Tremoy et al., 2011), but it was found to greatly attenuate the water isotopic signals (Sturm and Knohl, 2010; Griffis et al., 2010; Schmidt et al., 2010; Tremoy et al., 2011) ~~(cite?)~~. Testing in various labs has led to the adoption of plastic or metal tubing, but the details of the experiments and results are ~~sparce~~sparse (Sturm and Knohl, 2010; Griffis et al., 2010; Schmidt et al., 2010; Tremoy et al., 2011; Steen-Larsen et al., 2014). Commonly used tubing material types now include copper (Steen-Larsen et al., 2014) and several types of plastic including polytetrafluoroethylene (PTFE, commonly referred to as Teflon) (Sturm and Knohl, 2010; Griffis et al., 2010), perfluoroalkoxy (PFA) (Schmidt et al., 2010; Tremoy et al., 2011), fluorinated ethylene propylene (FEP) (Luo et al., 2019), and high-density polyethylene (HDPE) (Griffis et al., 2010). Fluorinated polymers (FEP, PFA, and PTFE) are commonly used as transfer lines in chemical, pharmaceutical, food processing, and oil and gas industries because of their chemical- and weather-resistance, as well as their non-stick and dielectric properties (Chemours, 2018). These materials have found favor in water vapor isotope applications for the same reasons.

Air tubing choices are important because materials may have different affinities, or degree of attraction, for the isotopologues of water. This affinity causes a delay in the speed at which the isotopologue signals move through the tubing due to exchange rates with water molecules stuck to the walls, called the memory effect. The memory effect is strongest for δD compared to $\delta^{18}O$ due to the stronger hydrogen bonding of the molecules containing deuterium slowing tubing wall exchanges (Sturm and Knohl, 2010; Griffis et al., 2010; Schmidt et al., 2010). This can result in false d~~D~~euterium-excess (D-excess, defined as $\delta D - 8 * \delta^{18}O$) anomalies and is important to minimize when D-excess signals are interpreted as fast temporal-scale atmospheric signals (Managave et al., 2016; Galewsky et al., 2016; Sodemann et al., 2017; Salmon et al., 2019). Memory may be lessened at higher temperatures and faster air flow rates (Griffis et al., 2010; Pagonis et al., 2017).

It is important to minimize isotopic wall effects in the intake tubing lines and other in-line elements positioned before the analyzer to minimize signal attenuation. Five~~our~~ studies previously reporting memory effects of tubing types tested a maximum of three materials at a time and are summarized in Table 1 (Sturm and Knohl, 2010; Griffis et al., 2010; Schmidt et al., 2010; Tremoy et al., 2011; Steen-Larsen et al., 2014). Most concluded that Dekabon was not suitable for water isotope applications but varied in which tubing was preferred across applications. The National Ecological Observatory Network (NEON) selected FEP for their monitoring installations which has not been widely used in reported studies (Luo et al., 2019). In this study, we tested five of the commonly used and reported best tubing types under nearly identical conditions at two different temperatures to determine which tubing type and temperature combination results in the smallest isotopic signal attenuation. We also tested Bev-A-Line XX, a commonly used tubing material in soil gas studies.

Formatted: Not Highlight

Table 1. Literature findings

Author, year	Materials Tested	Isotopes Used/Goals	Result
*Schmidt et al. 2010	Stainless steel, PFA, and Dekabon	δD and $\delta^{18}O$, Analyzer calibration	PFA better than SS. Both better than Dekabon.
*Sturm and Knohl 2010	PTFE and Dekabon	δD and $\delta^{18}O$, Analyzer characterization	PTFE better than Dekabon
Griffis et al. 2010	"Natural colored" HDPE, Teflon (PTFE), and Dekabon	δD and $\delta^{18}O$, $\delta^{18}O$ measurements of evapotranspiration in eddy covariance setups	HDPE equal or slightly better than PTFE. Both much better than Dekabon.
Tremoy et al. 2011	PFA and Dekabon	δD, $\delta^{18}O$, and D-excess, Analyzer characterization and D-excess measurements	PFA better than Dekabon
*Steen-Larsen et al. 2014	Copper, stainless steel, and PTFE	δD, $\delta^{18}O$, and D-excess, environmental controls on D-excess measurements	Copper better than both.

*Indicates experimental details and results of source-switching experiments are included in the peer-reviewed published materials.

2 Methods

In this study, we tested PFA, FEP, PTFE, HDPE, and copper at ambient and elevated temperatures using self-regulating heat tape. We switched between two isotopically distinct vapor sources to examine memory effects during water vapor stable isotope measurements. We also tested Bev-A-Line XX at ambient temperature.

2.1 Analyzer

A Los Gatos Research, Inc. (LGR) Triple Water Vapor Isotope Analyzer (TWVIA) Off-Axis Integrated-Cavity-Output Spectroscopy system (OA-ICOS) ~~analyzer~~ was used for testing. The air flow rate through the analyzer was 0.635 ± 0.006 ~~1~~ L min^{-1} ~~(slow analyzer) or 0.2-0.3 L min^{-1} (fast analyzer)~~ run in standard mode at ~40 Torr.~~.~~ The analyzer precision was characterized over 18 hours at approximately 9,300 ppm.~~.~~ The ~~20s average~~ Allaen deviation ~~is~~ at two ~~Twenty --~~seconds ~~averaged one-sigma values~~ for δD and $\delta^{18}O$ ~~δD and $\delta^{18}O$ at the slow analyzer speed with in-line elements~~ was approximately~~re~~ ~~10~~.34 ~~0.5~~‰ and 0.1~~4~~58 ~~2~~‰, respectively (Fig. S1, Guerrier et al., 2020)~~,~~ ~~over 184.5 hours at approximately 98,3800 ppm.~~ ~~While it's customary to average the data over an interval to improve precision, we did not apply a running mean to our signal transition to preserve the original sweepout speed and artificially~~ In order to preserve the attenuation curve resolution, no running mean was applied to the δD and $\delta^{18}O$ data. However, a two second averaging interval is the lowest time limit of the Allan deviation code output (Guerrier et al., 2020), so two second averaged Allan deviation values are reported. An Allen deviation plot of analyzer variance (Fig. S14, Guerrier et al., 2020) estimates a two second averaged D-excess precision better than ± 3~~1~~.35 ‰, and a 10 s average better than ± 1.0 ‰.~~ For the fast analyzer without in-line elements, these values were 0.3‰ for δD and 0.10‰ for $\delta^{18}O$ over 2.3 hours at ~9,200 ppm.~~

Formatted: Indent: First line: 0"
Formatted: Not Highlight
Formatted: Highlight
Formatted: Not Highlight
Formatted: Not Highlight
Formatted: Not Highlight
Formatted: Not Highlight
Formatted: Not Highlight
Formatted: Not Highlight
Formatted: Not Highlight
Formatted: Not Highlight
Formatted: Not Highlight
Formatted: Not Highlight
Formatted: Superscript
Formatted: Not Highlight
Formatted: Not Highlight
Field Code Changed
Formatted: Not Highlight
Field Code Changed

2.2 Experimental Setup

The memory effect of the tubing material was tested by switching between two sources of moist air with different isotopic values but nearly identical water vapor mixing ratios (~9,2000 ppm.) (Table S1). We chose to hold water vapor mixing ratios constant to minimize additional effects of moistening and dehydrating the tubing walls, but rather isolate any differences in the rate of exchange of the isotopologues. It also eliminated the need to calibrate to correct the isotopic measurements for the mixing ratio dependence of the analyzer. A LiCor model LI-610 portable dew point generator (DPG) was used to create a vapor of approximately -187 ‰ δD, -25.6 ‰ $\delta^{18}O$, and 17.4 ‰ -170‰ δD, -21.3‰ $\delta^{18}O$, and -1.8‰ D-excess, measured by the analyzer, from water at 5 degrees°C for the slow analyzer tests. The second vapor of approximately -31.8 ‰ δD, -5.7 ‰ $\delta^{18}O$, and 14 ‰ -34‰ δD, -3.7‰ $\delta^{18}O$, and -3.2‰ D-excess was produced by a Los Gatos Research Water Vapor Isotope Standard Source (WVISS) for the slow analyzer tests. For the fast analyzer tests, these values were approximately -179‰ δD, -22.1‰ $\delta^{18}O$, and -1.5‰ D-excess from the DPG and approximately -27‰ δD, -3.1‰ $\delta^{18}O$, and -2.8‰ D-excess from the WVISS. DPG-generated vapor isotopic values for the experiments became isotopically enriched over time as water evaporated from the liquid reservoir following Rayleigh fractionation. Isotopic δD and $\delta^{18}O$ δD and $\delta^{18}O$ transitions were normalized to a 100 to 01 scale to compare across experiments and adjust for source water and analyzer drift over time. Five replicate switches were completed for each experiment where the vapor sources switched approximately every 64 minutes giving sufficient time to reach a new isotopic equilibrium. We present data through 20 minutes as equilibrium was already established (with the exception of Bev-A-Line XX).

For each experiment, the WVISS programming and internal valve system controlled the switching between the DPG output connected to the WVISS inlet port and the WVISS (Fig.ure 1) output to the TWVIA. The WVISS was connected to the analyzer by to the inlet protectoranalyzer by by approximately 100 fooeet (~30.5 m, lengths listed in S1Table S1) long sections of 1/4 in.ch (6.35 mm) outer diameter (OD) test tubing for the main experiments. The inlet protector is a ~3 inch (~7.6 cm) piece of thick-walled FEP with a stainless steel Swagelok union used to prevent damage to the inlet of the analyzer itself, but this protector is not expected to affect the results significantly. The Swagelok connection to the analyzer included an extra stainless steel union and ~2.53 -in.ch (~67.46 cm) thick-walled FEP to protect the bulkhead union threads from wear during the experiment, but this addition is not expected to affect the results significantly. AdditionalOther tests were done with a two short (62 in.ch or 1.57 m) and a long (99 feet 1/2 in.ch or 29.75 m) pieces of thick-walledf PTFE FEP(53 inch or 1.35 m thick-walled PTFE; 54 inch or ~1.37 m thin-walled PTFE) to quantify sensitivity to tubing length and interior diameterinner volume. Tubing inner diameters (ID, summarized in Table S1) were 3/16 in.ch (~4.76 mm) with the exception of HDPE and, thick-walled FEP, and thick-walled short PTFE, which were 1/8 in.ch (~3.18 mm) ID. The thin-walled FEP tubing was pieced together using three stainless -steel Swagelok unions, but this is not expected to affect the results significantly.

Tubing and self-regulating heat tape (EASYHEAT ADKS-0500, 100 -foot (~30.5 m) roof and gutter de-icing kit) were wrapped in either flexible foam tape (HDPE, PTFE, thick-walled FEP; AP/Armaflex TAP 18230 insulation tape) or rigid foam pipe insulation (copper, thin-walled FEP, PFA; Tundra brand 1/2 in.ch or 1.27 cm wall). The thermocouple probe was placed inside the insulation on the side of the ttested tubing opposite of the heat tape, ~3about three inches (~7.6 cm)" from the end of the heat tape closest to the analyzer inlet. A datalogger recorded the

Formatted: Not Highlight
Formatted: Highlight
Formatted: Highlight
Formatted: Highlight
Formatted: Font: Font color: Auto, Not Highlight
Formatted: Font: Font color: Auto, Not Highlight
Formatted: Font: Font color: Auto
Formatted: Font: Font color: Auto
Formatted: Not Highlight
Formatted: Highlight

average temperature over the ~10- hour experiments. During heated tubing tests, the tubing was allowed to warm up at least an hour to ~ 60°C prior to measurements to let the tubing moisture equilibrate to the elevated temperature and minimize the effects of degassing water molecules adhered to the tubing from previous experiments. Differences in the insulation properties of the two materials used and likely differences in thermocouple placement relative to unavoidable gradients in temperature resulted in differences in aAverage temperatures for each experiment, ranging from 48.6 to 75.2 °C are listed in (Table S1).- All heated experiments (average 60 ± 8 °C) are significantly warmer than ambient temperature experiments (average 24 ± 1 °C).

Aan external pump (KNF pump, model N920-2.08) was added to the TWVIA to pulls air through the analyzer at the maximizeum air flow ratethe turnover rate of air inside the analyzer. The TWVIA itself regulates the outflow to maintain a constant internal pressure, resulting in discontinuous (jumpy) flow rates which averaged 0.635 ± 0.006 L min^{-1}. This air flow rate led to an analyzer mean residence time (referred to as residence time) of 3.97~4 s. Temperature adjusted Calculated test tubing residence times were 1.0 ± 0.09 s 1.2 s for short thick-walled FEP, 19.7 ± 1.6 s22.7 ± 0.2 s for long thick-walled tubing, and 45.2 ± 2.5 s 50.8 ± 0.8 s for long thin-walled tubing. –The test tubing was placed between the WVISS and the TWVIA. Switching between constant isotopic sources, WVISS and DPG, was controlled by the LGR software and valves inside the WVISS unit.

Formatted: Font: 10 pt, Font color: Text 1

Formatted: Indent: First line: 0.19"

Formatted: Default Paragraph Font, Font: (Default) Times New Roman, 10 pt, Font color: Black, Pattern: Clear

Formatted: Default Paragraph Font, Font: (Default) Times New Roman, 10 pt, Font color: Black, Pattern: Clear

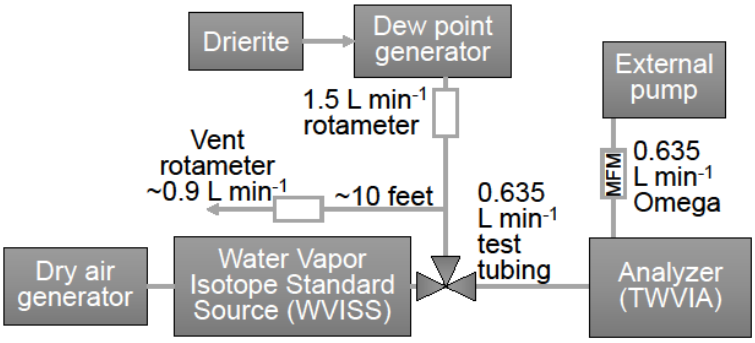

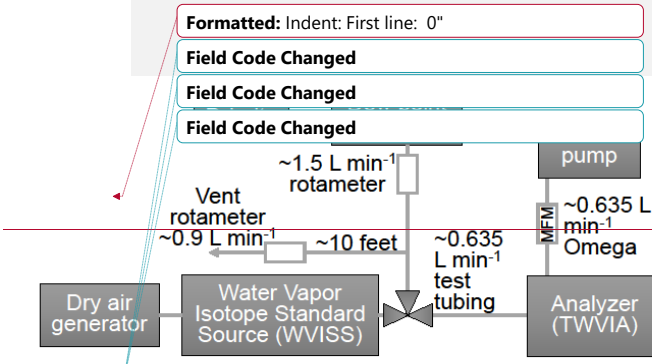

obvious

2.3 Data Processing~~Analysis~~

Isotopic values were measured at 1 Hz. No calibration to assign values to the international scale was performed on the isotopic measurements because the transitions were normalized to their starting and ending equilibrium values, resulting in signal transitions from ~~0~~0 to 1. Isotopic measurements by this analyzer are known to vary with water mixing ratio and potentially drift over long periods of time. Keeping water mixing ratios nearly constant eliminated the need to perform water mixing ratio corrections. Likewise, normalizing the measurements between sources as described below removed any potential influence of instrument ~~drift~~ or source drift over periods of more than 20 minutes.

~~Isotopic values were measured at 1 Hz and a 20 s running mean was applied to D-excess to reduce noise while minimizing smoothing over signal changes (Figure S1). This was done prior to normalization of the y axis for comparison between tubing types.~~ For δD and $\delta^{18}O$ ~~δD and $\delta^{18}O$~~, the ~~individual~~individual transitions from WVISS-to-~~/~~DPG (DPG-to-~~/~~WVISS) were normalized from 1~~0~~ to 0 (0 to 1)~~1~~ and then 5 replicates were averaged to characterize the transition memory~~s~~. ~~data was normalized to represent the enriched (maximum delta value set to, or 1) to depleted (minimum delta value set to, or 0) transition. Results from the depleted to enriched switch (where minimum delta value = 1 for easier visual comparison between switch directions) are presented in Figures S1 and S2. Maximum~~Initial δ~~δ~~ values were the average of 5~~10~~ seconds on either side of the maximum (minimum) value during the lag interval ~~before the~~ signal transition reaches the analyzer. ~~and the average minimum~~~~f~~Final δ~~δ~~ values were the average of measurements ~~over~~ 6~~18~~00–12~~0~~00 seconds after the source switch. In the ~~the fast analyzer~~ experiment with short th~~in~~ick-walled~~k~~ FEP ~~PTFE (where the lag time, discussed later in the methods, is 0 seconds)~~ the maximum (minimum) δ value was used due to the speed of the signal transition (i.e. no 1~~2~~0- s~~ee~~ average was used). D-excess was calculated as $\delta D - 8* \delta^{18}O$ ~~$\delta D - 8*\delta^{18}O$~~. D-excess was not ~~without normalization~~~~normailized~~normalized in the same way as δD and $\delta^{18}O$ ~~δD and $\delta^{18}O$~~ because the shape of the attenuation curve is different. A 10 -s~~ee~~ running mean was applied, and the 5 replicates were averaged. Replicates were screened based on successful WVISS-to-~~/~~DPG and DPG-to-~~/~~WVISS switching and consistent water vapor

Formatted: Indent: First line: 0"
Field Code Changed
Field Code Changed
Field Code Changed
Formatted: Font Alignment: Auto
Formatted: Not Highlight
Formatted: Not Highlight
Formatted: Not Highlight
Formatted: Font: Font color: Auto
Formatted: Indent: First line: 0.19"
Formatted: Font: (Default) Times New Roman
Formatted: Not Highlight
Formatted: Not Highlight
Formatted: Not Highlight
Formatted: Not Highlight
Formatted: Font: Font color: Auto
Formatted: Superscript
Formatted: Superscript

emixing ratios oncentrations ensuring that vapor source generators were operating properly. Only one replicate was discarded from
210 hehadPFA,afteranalysisthinPTFEexperimentwhentheDatawasdeletedafterReplacedtowatermixingconcentrationvaidityfromtheWVISS.Wecalculatedtheaverage D-excessδ value over 6340012360 0 seconds after the source switch and subtracted that value from all data points to adjust for small changes in D-excess source waters between replicates, especially in the DPG vapor which undergoes evaporative enrichment. Thesе 600–1200 seconds after the source switchs visually appear to be conditions of tubing equilibration and were used to calculate source vapor sample averages given in Table S1 and
215 summarized in Ssect.tion 2.2.

The replicates of each experiment were averaged to produce the curves in Figure 2. From this average of replicates, attenuation time thresholds were calculated and time-varying standard deviation was used to report uncertainty of the thresholds. This standard deviation was added or subtracted from the averaged curve to calculate the range of attenuation time uncertainty (supplemental excelFigure 3). This average of replicates was also used to
220 calculate the max peak metric for D-excessWhen comparing experiments betweenfrom different tubing lengths and IDs, differences in the internal volume result in different tubing residence times due to advection. The flow in all experiments was laminar with Reynold's numbers calculated between 579XX and 870XX. In Ssect.ion 3.1 XX.X we describe how the experiments are delay-lagg-adjusted to compare transitions directly. , as well as in the impulse response method (Steen-Larsen et al., 2014; Jones et al., 2017; Kahle et al., 2018) discussed in section 2.4.2.

225 Memory aAnalysis focuses oninclded both directions of the isotopic switchly on the isotopically enriched-to-depleted switch due to an isotopic signal artifact in the depleted-to-enriched switch created by pressure changes in the system during a purge cycle when the WVISS interval initiates. However, we did not see a difference in the overall conclusion attenuation times in either direction. Isotopically enriched-to-depleted (WVISS-to-/DPG) figures are presented in the main body of the text, and isotopically depleted-to-enriched (DPG-to-/WVISS) transitions are
230 available in the supplemental information (Figures. S2S1S23 and S2S43). While Aemisegger et al. (2012) found the enriched-to-depleted switch exhibited longer attenuation times, this was likely due to the change in water vapor mixing ratio of the sources in their experiment which did not occur here.

2.4 Memory Quantification Data Analysis

Our measurements allow us to quantify the tubing memory, adjusting for signal locationag time (calculated in Sect.
235 2.4.2). Memory effects are analogous to a low-pass filter (e.g. Zannoni et al., 2022) and signal transition shapes have been mathematically described in two general ways. The first, asPrevious studies have approximated the smoothing of a step-change input witas an h an approximately exponential transition and report a threshold time to some percentage of completion like an e-folding (63 %), 90 %, or 95 %or otherwise used threshold metrics based on an exponential time constant (Sturm and Knohl, 2010; Schmidt et al., 2010; Aemisegger et al., 2012; Steen-Larsen et
240 al., 2014)(Sturm and Knohl, 2010; Schmidt et al., 2010; Aemisegger et al., 2012) or log-normal transition (Steen-Larsen et al., 2014) in the source switch determined from a normalized source switching experiment(Sturm and Knohl, 2010; Schmidt et al., 2010; Aemisegger et al., 2012). These threshold metrics, such as e-folding time, indicate the time taken to reach a certain percentage of completionIn some cases, the threshold metrics were obtained from the data directly (Sturm and Knohl, 2010; Steen-Larsen et al., 2014)(cite Sturm and Steen-larsen) and

Formatted: Highlight
Formatted: Not Highlight
Formatted: Not Highlight
Formatted: Not Highlight
Formatted: Not Highlight
Formatted: Not Highlight
Formatted: Font: Times New Roman
Formatted: Font: Times New Roman
Formatted: Font: Times New Roman
Formatted: Font: Times New Roman
Formatted: Font: Times New Roman
Formatted: Font: Times New Roman
Formatted: Font: Times New Roman, Not Highlight
Formatted: Font: Times New Roman
Formatted: Font: Times New Roman, Not Highlight
Formatted: Font: Times New Roman
Formatted: Font: Times New Roman, Not Highlight
Formatted: Font: Times New Roman, Not Highlight
Formatted: Font: Times New Roman, Not Highlight
Formatted: Font: Times New Roman, Not Highlight
Formatted: Not Highlight
Formatted: Indent: First line: 0"
Formatted: Not Highlight
Formatted: Not Highlight
Formatted: Highlight

in others it appears an exponential function was fit to the data first and the metrics were extracted from the fit (Schmidt et al., 2010; Aemisegger et al., 2012)~~(cite Schmidt and Aemisegger).~~ ~~The~~A second method used in the literature ~~starts with a function describing the normalized transition similar to above, but a function based on the~~takes the first derivative of the normalized transition (Steen-Larsen et al., 2014) ~~is also applied~~and characterizes an impulse response function using curve fitting (Jones et al., 2017; Kahle et al., 2018)~~(2014)(2017)(Jones et al., 2017; Kahle et al., 2018)(2018). (2017)~~We have quantified memory effect metrics using ~~both of these~~both methods.~~E-folding time~~

2.4.1 ~~$t_{63\%}$, $t_{95\%}$, $t_{3\%_{eq}}$ and maximum D-excess peak metrics~~Threshold metrics

~~Once data is normalized (as previously described),~~ We extracted attenuation threshold metrics ~~such as e-folding time and $t_{95\%}$ can be extracted~~directly from the normalized and replicate-averaged data (not an exponential fit). An e-folding time corresponds to τ =1/e of the signal transition remaining to reach a new value. In this study, we have chosen to estimate attenuation threshold times at ~~approximately~~ 1τ (~63 %) and 3τ (~95 %) completion of the switch to the next δD and δ^{18}O~~δD and δ^{18}O~~ value, denoted as $t_{63\%}$ or $t_{95\%}$ respectively (Schmidt et al., 2010). These t values are ~~as~~ the time the averaged curve intersects the threshold percent value. ~~–~~We chose not to fit exponential curves to extract an e-folding time, because the measured attenuation curves ~~follow more of a reverse sigmoidal shape~~ were not accurately described by an exponential curve (not shown). The 1 ~~-~~standard deviation envelope was calculated by taking the standard deviation of the 5 replicates at each time step. Errors associated with ~~these values of~~ attenuation_threshold times were determined~~calculated~~ by finding the time ~~after switch~~ that the 1~~-~~ standard deviation envelope of the averaged replicates ~~normalized and average curve +/- standard deviation reached~~intersects the completion threshold. ~~Signal propagation is also delayed by the time it takes air to move through the tubing from the WVISS and mixing inside the analyzer, denoted as lag time. Lag time is controlled by the air flow rate through the instrument and optical cavity size, and intake tubing ID and air flow rate (Schmidt et al., 2010).~~Data ~~(supplemental excel) presented has been location adjusted.~~

D-excess signals of the source transitions ~~have a very different shape~~are not unidirectional and memory must be quantified differently. Previous studies reported that δD~~δD~~ signals take longer to equilibrate with the surface of tubing materials compared to δ^{18}O~~δ^{18}Od18O~~ signals due to ~~interactions~~ isotopic effects of hydrogen binding with the tubing walls ~~and hydrogen bonding compared to δ^{18}O signals~~ (Sturm and Knohl, 2010; Griffis et al., 2010; Schmidt et al., 2010; Aemisegger et al., 2012). The D-substituted hydrogen-bonds exchange with the vapor more slowly. This difference leads to a D-excess transition that ~~is not a monotonic near-exponential transition like δ^{18}O and δD, but rather~~ has a transient ~~positive~~ anomaly until the δD~~δD~~ signal propagation catches up to the δ^{18}O ~~δ^{18}O~~ signal. The direction of the D-excess transient peak depends on the direction of the isotopic signal switch. In the enriched-to-depleted transition, the enriched δD signal is retained on the tubing walls creating a transient, positive anomaly in D-excess while approaching equilibrium. However, in a depleted-to-enriched transition, the depleted δD signal has been preserved on the tubing walls creating a negative D-excess anomaly during isotopic equilibration. ~~The average difference between the beginning and ending D-excess values was only 1~~4.0.4‰ ~~for both fast and slow analyzer settings, while the transient peaks reached up to ~~2~~20‰ for slow analyzer air flow and ~15‰ for fast~~

Formatted: Not Highlight

Formatted: Font: Not Italic, Not Superscript/ Subscript

Formatted: Indent: First line: 0"

Formatted: Font: Italic

Formatted: Font: Italic

Formatted: Font: Italic

Formatted: Not Highlight

Formatted: Not Highlight

Formatted: Not Highlight

analyzer air flow. The absolute value of the maximum transient peak (|maximum transient peak|) values wasere identified (supplemental excel) and associated errors are given as the standard deviation of the time of the maximum peak (SITable S2). The direction of the D-excess transient peak depends on the direction of the isotopic signal switch. In the enriched-to-depleted transition, the enriched δD signal is retained on the tubing walls creating a transient, positive anomaly in D-excess while approaching equilibrium. However, in a depleted-to-enriched transition, the depleted δD signal has been preserved on the tubing walls creating a negative D-excess anomaly during isotopic equilibration. An e-folding time value cannot capture the features of the D-excess transitions. The metric threshold chosen to measure completion in D-excess transitions is a 3 ‰ threshold within the new equilibrium value ($t_{3‰}$), determined by the average over 6340012360000 s. This threshold is a conservative threshold ofestimate of analyzer precision of D-excess measurements if δD δ□D precision was 1.0 ‰ permil and $\delta^{18}O\delta^{18}O$ d18O precision was 0.25 ‰permil. An Allen plot of the slow analyzer variance estimates D-excess precision better than of ± 1.5 ‰ (Figure S421) (Fig. S4, Guerrier et al., 2020)), while fast analyzer variance estimates ±1.1‰.

2.4.2 Impulse response method

Similar to above, data must be normalized, and then a transfer function needs to be applied prior to further interpretationIn the impulse response is method, we take advantage of the first derivative of the observationsobserved attenuation curves to clearly identifying the timing and rates of change. To decrease the noise in the first derivative, it's necessary to reduce noise in the observed attenuation curves. In previous studies, noise reductionthis is achieved by fitting a smooth transfer function to the observations. Jones et al. (2017) and Kahle et al. (2018), used a lognormal times* lognormal (log-log) function recreatesto fit the data, while in Steen-Larsen et al. (2014) only one lognormal iss used. For our attenuation curves, neither these fits were not appropriatea single or double log-normal fit the observed data well. Our data was most accurately recreated by a transfer function of the form in lognormal * lognormal * normal fit (Eq.uation (1), (with the exception of the depleted-to-enriched transition for HDPE where an additional normal fit was addedused):.

$$\delta_{transfer}(t) = c_1 * \left[1 + erf\left(\frac{log(t)-\mu_1}{\sigma_1\sqrt{2}}\right)\right] * \left[1 + erf\left(\frac{log(t)-\mu_2}{\sigma_2\sqrt{2}}\right)\right] * \left[1 + erf\left(\frac{t-\mu_3}{\sigma_3\sqrt{2}}\right)\right] + c_2$$

Equation (1)

where t is time from the normalized average of replicatessince switching, σ is the location of each log/normal, μ is the standard deviation of each log/normal, and c_1 and c_2 are scaling factors. The values of σ_1, σ_2, σ_3, μ_1, μ_2, and μ_3 are optimized by least squares minimizing the squares of errors using the "DEoptim" global optimization function in the R package of the same name (Ardia et al., 2022). The form of the fitting model here is not that important as long as the observation featuress are faithfully retained produced in the smooth curve fit, as seen in Fig.ure 2a panel a.

Once a transfer function is fitted, the first derivative of the transfer function is calculated to obtain the impulse function. ThisWe fit the first derivative is then modeled by anthe impulse function fitted by the model in (Eq.uation (2) based on a skew-normal function added to a normal gaussian function. (R Core Team, 2023)

Formatted: Not Highlight
Formatted: Not Highlight
Formatted: Font: Font color: Black
Formatted: Font:
Formatted: Indent: First line: 0"
Formatted: Left
Formatted: Font: Italic
Formatted: Font: Italic
Formatted: Font: Italic
Formatted: Font: Italic
Formatted: Not Superscript/ Subscript
Formatted: Font: Italic
Formatted: Font: Italic
Formatted: Font: Italic, Subscript
Formatted: Font: Italic
Formatted: Font: Italic, Not Superscript/ Subscript
Formatted: Font: Italic
Formatted: Font: Italic
Formatted: Indent: First line: 0.25"

$$\delta_{impulse}(t) = \left(c_1 * \left[\left(\frac{\log 1}{\sqrt{2\pi}}\right) * e^{\frac{-x_1{}^2}{2}}\right] * \left[\frac{1}{2} + erf\left(\frac{x_1 * \log \alpha}{\sqrt{2}}\right)\right]\right) + \left(\left[\left(\frac{1}{\sqrt{2\pi}}\right) * e^{\frac{-x_2{}^2}{2}}\right] * c_2\right) \quad \text{Equation (2)}$$

$$x_1 = \frac{(t-\xi)}{\omega} \quad \text{Equation (2.2)}$$

$$x_2 = \frac{(t-\mu_{\xi})}{\sigma_{\xi m}} \quad \text{Equation (2.3)}$$

where in the skew-normal terms, ξ is the location of the maximum impulse peak, α is shape, and ω is scale, t is time since switching, $\sigma_{m\xi}$ is the standard deviation of the additional PDF and μ is its mean, and c_1 and c_2 are scaling factors. In the skew-normal, ξ is the location, α is shape, and ω is scale. The variables are optimizedparameters are solved for using a two-step method: first by least-squares, again using the "DEoptim" function (Ardia et al., 2022) to narrow-down optimal variableprovide an approximate initial guess, and second values to a smaller range prior to utilizing the "nls" non-linear least squares function in the "stats" R package of base R (R Core Team, 2023) to provide parameter fine-tuning and error metricsuncertainty estimates for the outputs listed aboveof each parameter.

While Jones et al. (2017) was able to fit impulse functions of their data solely with a skew-normal PDF fit (a standard normal probability distribution function times a standard normal cumulative distribution function, or PDF * CDF), we most accurately reproduced the first derivative by adding an extra PDF (in Eq.uation (2) 4). Figure 2b panel b shows a comparison of the Jones et al. (2017) impulse function skew-normal fit compared to the impulse function fit we used in this studyin Equation 2. While ourOur impulse function model fits the model of the transfer function derivative, the Jones method does not accurately depict the memory tail in our experiments better than the skew-normal PDF model from Jones et al. (2017). (2017)

Formatted: Indent: First line: 0"

Formatted: Font: (Default) Times New Roman, Italic

Formatted: Font: (Default) Times New Roman

Formatted: Font: (Default) Times New Roman

Formatted: Font: (Default) Times New Roman, Italic

Formatted: Font: (Default) Times New Roman

Formatted: Font: (Default) Times New Roman, Italic

Formatted: Font: Times New Roman

Formatted: Font: Times New Roman, Italic

Formatted: Font: Times New Roman, Italic

Formatted: Font: Times New Roman, Italic

Formatted: Font: Times New Roman, Italic

Formatted: Font: Times New Roman, Italic

Formatted: Font: Times New Roman, Italic

Formatted: Font: (Default) Times New Roman

Formatted: Not Highlight

Field Code Changed

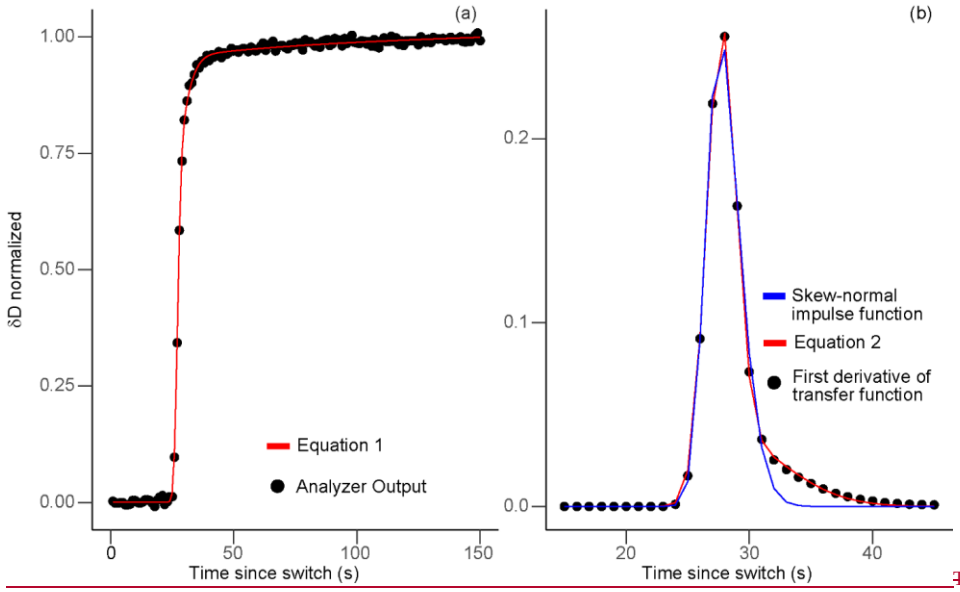

Figure 2. ~~Example~~ Example of model function fits for the unheated long thick-walled FEP experiment. Panel (a) compares~~ing~~ normalized and averaged ~~the~~ analyzer output (black dots) with the transfer function given in Eq.~~uation~~ (1) (red line). Panel (b) compares the impulse function derived from the first derivative of the transfer function fit ~~in Equation 1~~ evaluated every second (black dots), with the fit from~~from~~ Eq.~~uation~~ (2) (red line) and the skew-normal impulse function (blue line) used in Jones et al. (2017) and Kahle et al. (2018). ~~compared to the first derivative of the transfer function from the unheated long thick walled FEP experiment. While the red line (Equation 2) closely fits the data, the blue line (skew-normal) does not fit the memory tail.~~

~~To compare the attenuation curves across experiments, we adjuste~~

$$\beta = \frac{\alpha}{\sqrt{1+\alpha^2}}$$ ~~Equation~~ (3.1)~~5~~

$$\sigma_s{}^2 = \omega^2 * (1 - \frac{2\beta^2}{\pi})$$

~~Equation~~ (3.2)~~6~~

$$\sigma_s = \sqrt{\sigma_s{}^2}$$

~~Equation~~ (3.3)~~7~~

Formatted
Formatted
Formatted
Formatted
Formatted
Formatted
Formatted
Formatted
Formatted
Formatted
Formatted
Formatted
Formatted
Formatted
Formatted
Formatted
Formatted
Formatted
Formatted: Indent: First line: 0.25"
Formatted: Indent: First line: 0"
Formatted: Indent: First line: 0.5"

3.1 Comparison of residence, lag, and location times1

The residence time of air in the system is mathematically predicted using the tubing ID, length, temperature, pressure within the tubing, and –and air flow rate through the tubing –(Table S2?) and analyzer combined. ResidenceLag times are decreased by decreasing shortening the tubing length and inner diameter or increasing temperature and air flow rates through tubing and analyzer. Average l Observed lag times ((not shown) , from breakpoint analysis correlatespond well with predicted calculated lagresidence times (Fig.ure S12a panel a)). For the long thick-walled tubing, the calculated residence time lag isshould be approximately 19.7232.7 ± 1.60.2X s, with slight variations due to temperature and small length differences which agrees well with to observed lag of 23.1 XX± 1.2 X s. For long thin-walled tubing, the residence time is approximately 45.250.8 ± 0.82.5 s, and average lag times are is 53.0 ± 4.0 s. The largesthighest discrepancies between residence and lag times (< 12.59 s) are found in unheated copper and unheated PFA. These differences are partially due to the residence time of the analyzer (~4 s). The rest of the difference (< 5 s) may be due to variations in effective flow velocities for the thin-walled tubings or error in the breakpoint lag calculation. For short thick-walled FEP, the residence time is 1.0 ± 0.09 s 1.18 and average lag time is 1.5 ± 1.7 s. While residence times Overall, heated tubing lag and residence times were shorter than their unheated counterparts (Table S2?). are not expected to vary much with temperature, the heated tubing lag times were shorter than their unheated counterparts. While ,

Similarly, the location time parameter fitted using the impulse response method (discussed in Sect. 2.4.2) is the timing of the maximum peak of the impulse function (or the steepest portion of the attenuation curve, discussed in Sect. 2.4.2)curve. The location time is sensitive to the advection lag and the steepness of the isotopic transition. , and is nearly identical to the $t_{63\%}$ estimates from the experiments. Because of this relationship, location times correspond well with the observed lag times, the calculate lag times, as well as the $t_{63\%}$ times. Our estimated location time for the long thick-walled tubing (25.26 XX± 1.3X s, Table S2) matches the lag time calculated above when accounting for thee approximately or <<2 5 seconds between the initial signal change and the maximum slope of the attenuation curve (or peak in the impulse function). Because of this relationship, location times correlatedespond well well with the observed lag times (Fig.ure S21b panel ba) and, the residence times and are nearly identical to the unadjusted $t_{63\%}$ estimates from the experiments as well (Fig.ure S21 panel cb). The differences in location time between different tubing experiments is not fully explained by differences in residence time predictions. -The location time extracted from the δD impulse function is [illegible] experiments consistently showed a similar or shorter unadjusted –$t_{63\%}$ time in δD and $\delta^{18}O$ compared to their unheated counterparts (Fig.ure S21 panel d). -We suspect this is due to an increased speed of initial signal transition, as the elevated temperature has driven off some water molecules and there is less time required for full equilibration. as well as the $t_{63\%}$ times.

To more readily isolate identify differences in curve shape, we adjusted the attenuation curves to a common starting point by subtracting the fitted location time. This is similar to adjusting to You could have a paragraph describing differences in lag and/or location. The 'location' parameters match up extremely with the t63 efolding time, which makes sense to me. These should agree generally with calculated residence times from volume/flow

[illegible] of lag time and tubing temperatures which influence residence time, we decided the location time was the most [illegible]

Lag/location times were decreased by shortening the tubing length and inner diameter. The lag time can be mathematically calculated as the residence time of air in the sytem using the tubing ID, length, and air flow rate through the tubing and analyzer combined. Similarly, the location time parameter fitted using the impulse function method is the time of peak change, nearly identical to the t63% estimate from the experiments. For the long thick-walled tubing, the calculated lag should be approximately 23 +/- X s, with slight variations due to small length differences in 100 +/- X feet (~30.5 +/- X m). This matches our estimated location for the long thick-walled tubing when accounting for the <2 seconds between the initial signal change and the maximum slope of the attenuation curve (or peak in the impulse function). Heated experiments consistently showed a shorter location estimate. Care to comment on why?

The mean attenuation curves for the enriched-to-depleted transitions for all experiments (except short and long thick-walled FEP) are compared in Fig.~~ure~~s 3 and the depleted-to-enriched results are in ~~SI~~ Fig.~~ure~~ ~~, 4, S1~~S3~~2~~., ~~and~~ S22 Figures ~~start prior to 0 s because they~~ have been adjusted by the $\delta\delta^{18}O$ location time metric in order to more easily compare memory tails of the attenuation curves.~~,~~ T~~t~~herefore 0 s in these figures indicates the time of most rapid change in the transfer function and the peak of the impulse function. The δD signal was also $\delta\delta^{18}O$ location adjusted to highlight potential differences between the two isotopologues. ~~These results were used to compare tubing experiments and quantify $t_{95\%}$ and $t_{63\%}$ for δD and $\delta^{18}O$, or $t_{3\%}$ and |maximum peak| for D-excess which are summarized in the supplemental excelSI~~Figure 3. ~~Bev-A-Line XX immediately~~ stands out as the ~~worst~~ tubing material ~~type~~with the longest memory (Fig~~ures~~. 3 and ~~S1~~S2~~3~~). When normalized to start and end at "~~'~~true~~'~~" values assigned from a short thick-walled FEP test that occurred immediately prior, the Bev-A-Line XX never reached the 'true' value in either direction of the switch (Fig.~~ures~~ 3 and ~~S1~~S3~~2~~). There are slight variations within the rest of the tubing material type and temperature performances. ~~S, s~~pecifically, ~~when considering the~~ thin-walled FEP $\delta\delta$D (Figures 3, 4, S1, and S2).results show slower transitions compared to other tubing experiments. However, this separation is due to a larger location time difference~~ratio~~ between δD and $\delta\delta^{18}O$ for thin-walled FEP than the rest of the tubings. ~~However, there~~When adjusted for location,~~There is remarkable agreement between tubing types for δD or $\delta^{18}O$, and little-to-no consistent difference between~~ heated experiments often appear to have a ~~slower transition~~less steep δD slope and intercept the $t_{63\%}$ ~~t~~63 metric later than ~~and~~ unheated experiments. We see this specifically in the δD signal for all tubings in the enriched-to-depleted direction with the exception of long thin-walled FEP, and ~~we see this~~ for c~~C~~opper and ~~PTFE~~HDPE in the depleted-to-enriched direction. ~~xxxx and~~ Location adjusted attenuation curve slopes for~~in~~ $\delta^{18}O$ intercept the $t_{63\%}$ metric later~~earlier~~ and are shallower~~teeper~~ for the ~~un~~heated experiments for ~~for~~ PFA in the enriched-to-depleted direction and ~~and~~ PTFE and c~~C~~opper in the depleted-to-enriched direction ~~and HDPEyyyyy in the enriched-to-depleted direction~~ (Fig.~~ures~~ 3~~,~~ 4,and S3~~S1S2~~, ~~and~~ S2~~Figures 2 and 3~~). ~~Figures 32 and S1 compares all tubing material types at two temperatures from -5 s through 100 s over the full 1-hour experiment length (panels a, c, and e) and through 15 s the first 600 s after the source switch (panels b, d, and f). Figures start prior to 0 s because they have been adjusted by location (lag + a few seconds) in~~

Formatted: Font: Times New Roman

Formatted

Formatted: Not Highlight

Formatted: Not Highlight

Formatted: Not Highlight

Formatted: Not Highlight

Formatted: Not Highlight

Formatted: Not Highlight

Formatted: Not Highlight

Formatted: Not Highlight

Formatted: Not Highlight

Formatted: Not Highlight

Formatted: Not Highlight

Formatted: Not Highlight

Formatted: Font color: Auto, Not Highlight

Formatted: Not Highlight

Formatted: Not Highlight

Formatted: Not Highlight

Formatted: Superscript

Formatted: Not Highlight

Formatted: Not Highlight

Formatted: Not Highlight

Formatted: Not Highlight

Formatted: Not Highlight

Formatted: Not Highlight

δδD attenuation times were slower compared to δδ^{18}O. Figures 3 and S1S23 panels b and d also show the mean attenuation curves for the other isotopologue for direct comparison (orange curves).). In the enriched-to-depleted transition, propagation of the depleted δδD signal was delayed relative to the depleted δδ^{18}O signal (as shown by the orange lines in Figures 3 and S32 panels b and d), creating a transient positive anomaly in D-excess before equilibrating with the new vapor source isotopic values. D-excess attenuation times are typically much longer than the $t_{95\%}$ times for δδD or δδ^{18}O (Table S2). FFor D-excess, the overall transition response curves and times to achieve 3‰ within the final value are similar when considering the range of the absolute value of the maximum peak valueserror is considered, regardless of tubing type. There is some separation in D-excess between heated and unheated experiments of the same tubing type and temperature. Given differences in D-excess vdeuterium excess values between sources, we caution overinterpreting the maximum D-excess deuterium excess anomalies between experiments, as evidenced by the different starting points in Fig. 3e.D-excess attenuation times are typically much longer than the $t_{95\%}$ times for δD or δ^{18}O (Table S2). On average it took approximately 33 seconds for the transient anomaly to decay to within 3‰ of the ultimate equilibrium value after location adjustment. Bev-A-Line XX does not reach a 95% or 3‰ attenuation time threshold, but it does reach the $t_{63\%}$ for both δD and δ^{18}O within the hour long source switches, 56 and 34 minutes, respectively (off-scale in Figure 3).

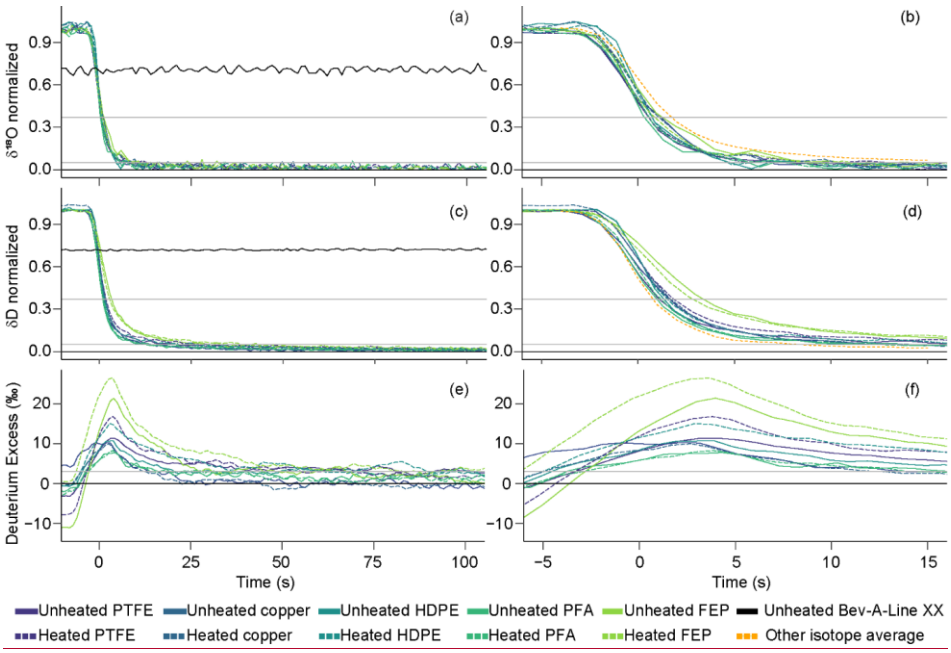

Figures 3 and S1 2, panels b and d also show the mean signal transition (starting at the location) for the other isotopologue in orangegrey for direct comparison showing the longer transition times for δD compared to δ^{18}O. For

Formatted: Not Highlight
Formatted: Not Highlight
Formatted: Not Highlight
Formatted: Not Highlight

Figure 32. Mean attenuation curves for enriched-to-depleted (WVISS-to-DPG) transitions of five replicates of each tubing type for $\delta\delta^{18}O$ (a, b), $\delta\delta D$ (c, d), and D-excess (e, f) plotted as approximate location adjusted time since source switch and location adjusted. The first column (panels a, c, and e) depicts time from -5 to 100 s the full 1-hour experiment length, while the second column (panels b, d, and f) depicts time from -5 to 15 s depict the first 600 s after the source switch. However, lines do not necessarily start or end at these values due to non-integer x-axis values. Solid lines indicate unheated experiments of thin-walled tubing, while dashed lines indicate heated experiments. For δD, $\delta^{18}O$, and D-excess, unheated and heated tubing performances are similar with no clear optimal material or temperature under these conditions. An orange grey curve in panel b shows mean $\delta\delta D$ for comparison with $\delta^{18}O$ in color and the orange grey curve in panel d shows $\delta\delta^{18}O$ for comparison with δD in color. To compensate for small differences in isotopic values between experiments, $\delta\delta D$ and $\delta\delta^{18}O$ δD and $\delta^{18}O$ are normalized from 10 01 with zero one at equilibrium with the first vapor source and zero1 at equilibrium with the second vapor source., and D-excess is adjusted to end at 0 ‰ over the same averaging time for each experiment. Gray horizontal lines indicate thresholds of 95 % and 63 % transition completion for $\delta\delta D$ and $\delta\delta^{18}O$, and 3 ‰ for D-excess, while a black line indicates 100 % equilibrium completion for all isotopes. Bev-A-Line XX is shown in panels a and c as a black line and never reaches a normalized 0 or 1 when compared to another the test run experiment immediately prior. Depleted-to-enriched results are presented in the supplemental, as there were no consistent and large differences in attenuation curves between source switching directions.

When testing differences in tubing temperature and dimensions dimensions and temperature using the same material, fin e transit time through the tubing, referred to here as lag time, like tubing length, and inner diameter, and effective flow velocities, do not appear to greatly influence the shape of the attenuation curve after location adjustment ($t_{\delta^{18}O}$, $t_{\delta D}$, and $t_{d\text{-}excess}$ values for location adjustment for δD, $\delta^{18}O$, $\delta\delta^{18}O$, and D-excess (Figures 3 4, S1, S2, and S3, S4). The short and long thick-walled tubing $\delta^{18}O$ and δD signals overlap each other (Fig. 4b and d), while the long thin-walled tubing has a shallower $\delta^{18}O$ slope (Fig. 4b) and a bigger delay between the δD and $\delta^{18}O$ signal transitions (Fig. 4d). n Because we've effectively normalized for tubing length, volume, and temperature through the $\delta^{18}O$ location adjustment, differences in the attenuation curve steepness could be attributed to vapor-wall interactions that are independent of bulk flow. The slight visual difference between short and long thick-walled FEP tubing lengths (Figure 4) do not seem to scale with length (5 feet vs 99 feet, or 1.6 m vs 30.2 m). Under these air flow conditions, the reverse sigmoid shapes of all isotopic transitions are similar. Nor do the slight visual differences between short and long or thick- and thin-walled or thick- and thin-walled FEP tubing lengths and IDs seem to scale with inner volume (0.01, and, 0.24, , and 0.53 L and 0.53 L for short thick-, and, long thick-, and long thin- - and long thin-walled tubings, respectively). EDiameters and effective flow velocities between thin- and thick-walled FEP doubled (6.1 to 13.8 ft. /s^{-1}, or 1.9 to 4.2 m/ s^{-1}), but this doubling was not reflected in the shapes of the isotopic attenuation curves. There is some stretching of the thin-walled FEP signal when compared to the thick-walled FEP in Fig ures 4 and S3 which could be due to the doubling of the ID and a reduction in the effective flow velocity. For δD, $\delta^{18}O$ δD, $\delta^{18}O$, and D-excess, unheated and heated tubing performances are practically similar, but present slight differences. These slight differences in temperature do not seem to follow a visual pattern. These s SWhile there are slight differences are

Formatted: Not Highlight
Formatted: Indent: First line: 0.25"
Formatted: Not Highlight
Formatted: Not Highlight
Formatted: Not Highlight
Formatted: Not Highlight
Formatted: Not Highlight
Formatted: Not Highlight
Formatted: Not Highlight
Formatted: Not Highlight
Formatted: Not Highlight
Formatted: Highlight

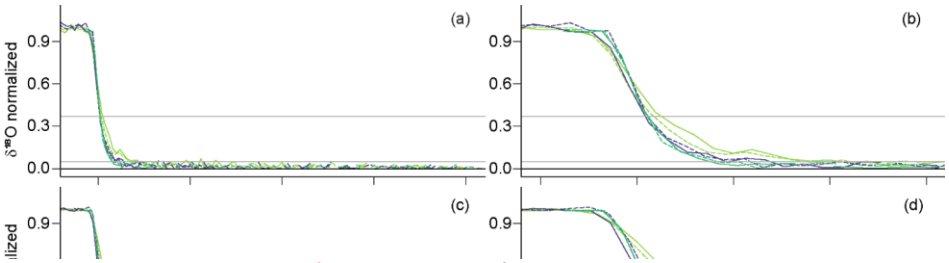

Figure 4. Mean attenuation curves for only FEP tubing for enriched-to-depleted (WVISS-to-DPG) transitions comparing tubing length and inner diameter for $\delta\delta^{18}O$ (a, b), $\delta\delta D$ (c, d), and D-excess (e, f) plotted as approximate time since source switch and location adjusted time since source switch. The first column (panels a, c, and e) depicts time from -5 to 100 s, while the second column (panels b, d, and f) depicts time from -5 to 15 s. Solid lines indicate unheated experiments, while dashed lines indicate heated experiments. For δD, $\delta^{18}O$, and D-excess, unheated and heated tubing performances are practically similar. While there are slight differences, this is generally within error of the experiments and noise of the analyzer. This leads us to conclude there is no clear optimal material or temperature under these conditions tested. To compensate for small differences in isotopic values between experiments, δD and $\delta\delta^{18}O$ δD and $\delta^{18}O$ are normalized from 10 01 with zero one at equilibrium with the first vapor source and zero 1 at equilibrium with the second vapor source, and D-excess is adjusted to end at 0 ‰ for each experiment. Gray horizontal lines indicate thresholds of 95 % and 63 % transition completion for $\delta\delta D$ and $\delta\delta^{18}O$, and 3 ‰ for D-excess, while a black line indicates 100 % completion for all isotopes. The location adjustment for the short tubing is much shorter than that of the long tubing, leading to a line

Formatted: Indent: First line: 0"

Formatted: Not Highlight

Formatted: Not Highlight

Formatted: Not Highlight

Formatted: Not Highlight

Formatted: Not Highlight

3.32 Qquantitative memory metrics

Quantitative metrics of σ_s, σ_m, $t_{95\%}$ and $t_{63\%}$ for δD and δδ^{18}O, or $t_{3‰}$ and absolute value of the ¦maximum peak¦ for D-excess were also used to compare tubing experiments (Table S2). The different memory metrics calculated via both methods (supplemental excel) provides a different order of "best" to "worst" tubing material types and conditions based on slight differences, though all tubings appear operationally similar (S1 Table S2). However, some common patterns emerge. According to Figures 34 and S1, as well as most impulse responsenearly all memory met metrics (σ_s and σ_m), short thick-walled FEP has the fastest attenuation impulse response time. The slowest(with the exception of heated long thick-walled FEP $\delta\delta^{18}O$ $\sigma_{m,ms}$ in the enriched-to-depleted switch direction). attenuation impulsesignal response response time for δδD is consistently found in the long thin-walled long FEP, while for $\delta\delta^{18}O$ the slowest signal responseattenuation impulse response times are found in unheated copper ($\sigma_{m,ms}$, enriched-to-depleted), unheated PFA (σ_{ms}, enriched-to-depleted), and heated PTFE (both metrics, depleted-to-enriched enriched-to-depleted depleted-to-enriched). In terms of residence time adjusted $t_{63\%}$ valuestimes, unheated copper is the worst and short thick-walled FEPheated PTFE is the best for both $\delta\delta^{18}O$ and δδD.For threshold metrics, Similarly, for $\delta\delta^{18}O$ residence time adjusted $t_{95\%}$ valuestimes are longest for unheated copper and shortest for short thick-walled FEP in both directions of the isotopic switch. For residence time adjusted δD $t_{95\%}$ times, long thin-walled FEP is the worst in the enriched-to-depleted direction while heated PTFE is the worst in the depleted-to-enriched direction. and sShort [illegible] consistently the best for $t_{3‰}$ and the absolute value of the ¦maximum D-excess peak¦ D-excess values, while heated long thin-walled FEP was the worse in both metrics in the enriched-to-depleted switch. In the depleted-to-enriched switch direction, heated PTFE was worse for $t_{3‰}$ butwhile for the absolute value of the ¦maximum D-excess peak¦ value in the enriched-to-depleted direction, heated long thin-walled FEP was the worste. memory metric used. Overall, heated memory metrics are generally either similar to or faster than those of the unheated memory metrics when comparing the same tubing types (Fig.gure S1d panel dSI Table). However, this this pattern does not hold for δD $t_{95\%}$, with differences of up to 15 s between heated and unheated PTFE, with unheated signal equilibrating faster.

Residence time adjustedThese attenuation threshold times, but as shown inare somewhat consistent with the visual analysis of Fig.ures 3, 4, S1S32, and S2S34., showing their performance was very similar. Unheated and heated attenuation curves andmemory metrics are generally similar (Figures 3,4,S1,S2, and supplemental excelSI Table). Memory tTimes are presented ares residence timelocation adjusted., as there is a correlation between location and residence time of tubing. With the location adjustment, Tthe measuredresidence time adjusted $t_{95\%}$ values for $\delta\delta^{18}O$ range from 6.93.86 11.22.819.3 seconds with an uncertainty of up to . Uncertainties range from less than 1 second to 3524 seconds for individual $t_{95\%}$ values. Measured values of $t_{95\%}$ for δδD range from 6.983 48138 seconds, with uncertainties of ranging from ~2 up to 1449 seconds. Because of the shape ofshallow slope of the attenuation curves at $t_{95\%}$ values contributing to large error estimates, we also report $t_{63\%}$ values also because they have smaller uncertainty estimates and may have a different sensitivity to tubing differences than the end of experiment tails. For our analyzer settings, residence time adjusted lag/location adjusted, $t_{63\%}$ values range from approximately 4.90.65 2.1 17.84.3 s and 1.60.7 14.32.7 s for both $\delta\delta^{18}O$ and δδD respectively, with uncertainty adding anotheron the order of one second to those ranges. $T_{63\%}$ vvalues are more similar between $\delta\delta^{18}O$ and δδD

Formatted: Normal, Left, Indent: First line: 0", Line spacing: single

Formatted ...

Formatted ...

~~from ‰ values (Figure S1 panels). Finally, residence time adjusted ‰ values for D-excess ($\delta^{2}H$ – 8 × $\delta^{18}O$ and adjusted because the isotopic anomaly for D-excess) range from 0.4–9.8‰ across while the main analyte, water vapor, ranged from ~15–37‰ and D-excess values typically ranged between ~0–30‰.~~ A model plot was manually digitized and superimposed over the data to help visualize the model's performance. We also did measured the distance from the absolute value of the maximum D-excess peak to 0‰, or the extent magnitude of the transient anomaly in D-excess signals. These values ranged from ~0–31‰, inclusive of error. The average difference between the beginning and ending D-excess values was 4.0 ‰. ~~, while the transient peaks reached up to ~ 30‰.~~

~~Similarly, we fitted a skew-normal impulse function to the data to quantify the response of D-excess to the step change in water vapor isotopic composition. We fitted the skew-normal impulse function to the data using the Levenberg-Marquardt algorithm in the Python package lmfit (Newville et al., 2014). We~~ We also calculated impulse response metrics for δD and $\delta\delta^{18}O$ using the skew-normal impulse function, were on average, longer for δD than $\delta\delta^{18}O$ and ranged from 0.6682–2.2 ± 0.02 s (Table S2). Mixing times (σ_{res}) from the skew-normal impulse function fit ranged from 1.46–5.9 ± 10.2 s and were also on average, longer for δD than $\delta\delta^{18}O$ ~~(supplemental excel SI Table S2)~~. Overall, impulse response metrics varied as expected for δD with length and volume with longer memory times for longer and larger volume tubing, but were inconsistent in $\delta\delta^{18}O$. ~~).~~ We were unable to calculate impulse response metrics for Bev-A-Line XX, as the isotopic switch was not achieved within the hour-long source switching. ~~Memory seems to present most in the σ_{res}, σ_{res}, $t_{95\%}$, and $t_{3\%}$ metrics based on their ability to identify changes at the lower portion of the impulse curve.~~

~~We see a temperature effect in mixing and pdf times and residence time adjusted metrics. Generally heated values are lower/faster.~~

Predictions of tubing material performance ~~under different sets of air flow conditions~~ can be made based on material properties. Hydrophobic materials that are nonpolar and have a high relative permittivity (also known as the dielectric constant, or a material's ability to prevent electrical fields from forming) are ideal for water vapor isotope studies as polar water molecules are affected by and can induce electric fields (Aemisegger et al., 2012). As previously ~~discussed~~shown, δD signal transitions~~s~~ are slowed ~~when traveling past the surface of a material when~~ compared to $\delta^{18}O$ signals, due to isotope-dependent ~~increased~~ hydrogen-bonding interactions with tubing walls. Limiting these interactions should lead to reduced isotopic attenuation times. Material s~~S~~pecifications vary by manufacturer and material purity, but in general, FEP and PTFE materials are expected to have the least amount of water absorption of the tubing types we tested (Table 2). Metals have a relative permittivity value of ~1 due to their sea of electrons, which in this case ~~move to~~ interact with the polar water molecules. Larger values of relative permittivity are better in this case, as water vapor molecules will be less attracted to the material. HDPE, FEP and PTFE have the highest ability to prevent electrical fields. FEP and PTFE may be expected to have the shortest isotopic attenuation times based on combined water absorption percentage and relative permittivity. However, at the air flow rate~~s~~ we tested, the memory metrics of FEP and PTFE were not ~~very~~ noticeably superior to the other tubing tested. ~~but might be confirmed by testing at lower air flow rates through intake tubing and faster analyzer internal flow rates.~~

Table 2. Material properties of tubing type options and their water absorption percentages and relative permittivity values.

Material	Water absorption % by tubing weight	Relative Permittivity (Dielectric constant) @ 1 MHz (ε_r)
FEP	<0.01[1]	2.1[2]

Formatted ...

Formatted: Font: Times New Roman

Formatted: Indent: First line: 0"

Formatted ...

PFA	<0.03[1]	2.05–2.06[2]
PTFE	<0.01[1]	2.0–2.1[2]
HDPE	0.10[1]	2.3–2.4[2]
Copper	N/A	~1
~~Stainless steel~~	~~N/A~~	~~~1~~

[1] after being submerged for 24 hours (ASTM D570). This metric is solely for plastic materials [2] (Electrical properties of plastic materials, 2021)

4 Discussion

Previous water vapor isotope studies have tried to identify suitable tubing material to use in sample inlets, and authors found several materials to be acceptable. To our knowledge, these materials had not be rigorously tested for wall adsorption/desorption effects leading to memory artifacts. Theory based on principles of gas chromatography and gas-wall partitioning predicts that the residence time of gases adsorbed on tubing walls is linearly proportional to tubing inner diameter and should decrease at higher temperatures as gas saturation concentrations changes (Pagonis et al., 2017). The experiments performed in this study begin to test these predictions for water vapor isotopes.

~~switch direction in the main paper?:~~While Aemisegger et al. (2012) found the enriched-to-depleted switch ~~exhibited longer attenuation times, this was likely due to the associated decrease in water vapor mixing ratio of the sources in their experiment which did not occur here.~~ ~~Important BUT not sure where to put it? Maybe in methods not instead/ wherever I talk about why we are only showing one switch direction in the main paper?:~~While ~~Aemisegger et al. (2012) found the enriched-to-depleted switch exhibited longer attenuation times, this was likely due to the associated decrease in water vapor mixing ratio of the sources in their experiment which did not occur here.~~

~~Memory seems to present most in the σ_{δ}, σ_{m}, $t_{95\%}$, and $t_{3\%}$ metrics based on their ability to identify changes at the lower portion of the impulse curve.~~

4.1 Effects of material and temperature

~~Our study compared five commonly used tubing materialtypes to determine whether material, and temperature, length, and diameter combinations differ in their isotopic memory effects. We also discuss the effects of intake tubing inner volumediameter and length, the inclusion of in-line elements including the filter and Omega mass flow meter, and analyzer air flow rates through the optical cavity on the attenuation time and shape of the attenuation curves.~~

Field Code Changed

Formatted: Font: Times New Roman, Font color: Black

Formatted: Font: Times New Roman, Font color: Black

Formatted: Font: Times New Roman, Font color: Black, Highlight

Formatted: Font: Times New Roman, Font color: Black, Highlight

Formatted: Font: Times New Roman, Font color: Black, Highlight

Formatted: Font: Times New Roman, Highlight

Formatted: Font: Times New Roman

Formatted: Normal

Formatted: Highlight

~~4.1 Effects of material type and temperature~~

~~at the temperatures~~, flow rate~~s~~, ~~and~~ humidity, ~~and temperatures tested~~, ~~and temperatures~~ (Fig~~ures 2 and~~ 3, ~~4, S1-S3~~2, ~~and S2-S4~~) ~~with the exception of Bev-A-Line XX~~. Our results are consistent with Griffis et al.'s (2010) assertation that HDPE is similar to PTFE. Similarly, Aemisegger et al., (2012) found little difference in attenuation times with varying PFA tubing temperatures. We were not able to replicate Steen-Larsen et al.'s (2014) finding that copper was better than PTFE. In our study, ~~;~~ ~~they~~tubing materials ~~performed similarly at the temperatures testes in our study~~ when comparing all memory metrics: σ_g, σ_m, $t_{g\%}$, ~~and~~ $t_{g\%}$, $t_{\%}$, and the absolute value of the ¦maximum D-excess peak¦. Variations in reported material properties presented in Sect 3.4 predict only slight differences in gas-wall effects in the commonly used tubing materials but were unable to explain the relative differences in memory metrics measured in these conditions. We believe the differences are too small to accurately measure in this experimental setup, partially based on the additional ~4 s residence time of the analyzer optical cell and internal plumbing.

Warmer temperatures are theoretically predicted to reduce attenuation times (Pagonis et al., 2017) by changing the saturation concentration of gases. The lower molar density of the warmer air means there is a shorter residence time through the tubing, increased molecular movement, faster wall exchanges, and fewer molecules stuck to the tubing walls. We found some evidence of this in comparing ~~fitted~~ location ~~-~~times and σ_m ~~sigma_m?~~ from the impulse function method (Table S~~1~~2~~?~~). Location times for heated tubings are always faster than their unheated counterparts, and σ_m values are similar to or shorter for heated tubings in most cases. Calculated residence times and observed lag times were also faster for heated tubings, but to varying degrees depending on the tubing. The heated tubing likely has faster residence, lag, and location times due to the decreased number of molecules in the tubing compared to the unheated experiment and possibi~~lit~~y also due to decreased wall effects.

Tubing residence time predictions are ~~—is~~ up to 12 s shorter than the measured breakpoint lag. ~~Uncertainities~~Uncertainties in tubing residence time (a few seconds~~xx~~), length (~~-~~a couple inches), and breakpoint lag (a few seconds) accounts for some of these differences. Tubing temperature measurements in the heated treatment varied depending on the position of the ~~thermistor~~ thermocouple relative to the heat cable. It is expected that the tubing was not at a perfectly uniform temperature, but we note that this heating design is commonly used in field conditions and represents likely inlet ~~behavior~~conditions. However, the lack of uniform temperature control leads to potential temperature~~-~~induced differences that are hard to quantify. This ~~is especially apparent~~should be considered when comparing residence time adjusted memory metrics between experiments. ~~There was also up to 12 s difference between lag and residence times. D~~These ~~d~~ifferences not attributed to ~~are partially due to the residence time of the analyzer (~4 s). The rest of the difference (~8 s) may be due to~~ variations in ~~effective flow velocities for the thin-walled tubings, variations in~~ temperature, length, ~~-~~ or error in the breakpoint lag may be due to ~~differences. Differences between~~ the bulk air flow and speed of isotopic change~~,~~ or wall effects. ~~While residence times varied based on temperature, the maximum temperature difference within our experiments (53.1 °C) would at maximum have a 7.4 s difference in residence time when considering the largest volume tubing (copper). Variations in reported material properties presented in Ssection 3.43 predict only slight differences in gas-wall effects in the commonly used tubing materials but were unable to explain the relative differences in memory response metrics measured in~~

Formatted: Not Highlight
Formatted: Not Highlight
Formatted: Not Highlight
Formatted: Not Highlight
Formatted: Not Highlight
Formatted: Not Highlight
Formatted: Not Highlight
Formatted: Not Highlight
Formatted: Not Highlight
Formatted: Not Highlight
Formatted: Not Highlight
Formatted: Not Highlight
Formatted: Not Highlight
Formatted: Not Highlight
Formatted: Not Highlight
Formatted: Not Highlight
Formatted: Not Highlight
Formatted: Not Highlight

~~these conditions. We believe the differences are too small to accurately measure in this experiment as it is partially based on the additional ~4 s residence time of the analyzer optical cell and internal plumbing~~

~~{paragraph on holding everything constant except length} We found that tubing dimensions, including inner volume and length, had small effects on the residual memory threshold metrics (Fig. 4 and S4) The tubing ID of the tubing affects the the residence, lag, and llag/location times, the surface area to air volume ratios, and the flow velocity past the surfaces well as the lag/location times. aAfter removing differences in residencelocation ag times in signal propagation to the analyzer based on tubing inner volume and the temperature influence on molecular density, we~~ [illegible] ~~short and long and short experiments was a factor of 1.97 (9.9 ± 0.0 ft/5.27 ft, or 3.02 m/1.6 m) which results in the same factor difference in. We did see an approximately 1.9x scaling factor in our~~ residence time calculations. The breakpoint lag differences between long and short thick-walled FEP tubing was approximately a factor of 8 times faster in the short tubing experiment. While there are slight differences in these memory metrics, this is likely due to the influence of the analyzer. Because the analyzer optical cavity and inner tubing has a residence time of ~ 4 sec, we are unable to resolve the residence time and memory metrics associated with the short FEP tubing (1.0 ± 0.09 s) only. Even with the large length difference, ~~, yet the T~~the shape of the isotopic attenuation curves remained similar ~~(~~after location adjustment which removes the length-based residence time differences ~~) remained similar~~ , ~~but slightly smearedpread out rather than smoothed~~ . ~~We see this when comparing thin-walled short and long tubing as well~~ (Fig.~~ure~~ 4 and ~~S2~~S43). ~~),~~ . ~~A 945% shorter length does not lead to a 95%similar decrease in Residence timeLlocation a adjusted tUnadjusted δD $t_{95\%}$95% and $t_{63\%}$ attenuation timesthreshold times for long thick walled FEP tubing we.re at maximum 5.434.2x and 41.861x greater than the nearly identical for the short, respectivelywhich matches theory as Pagonis et al. (2017) indicates isotopic attenuation does not scale with length and long FEP tubing.~~ Residence time adjusted δD $t_{95\%}$ and $t_{63\%}$ times for long thick-walled FEP tubing were at maximum 3.2x and 1.6x greater than the short, respectively. ~~–~~The mixing time scales (σ_s~~sigma s~~) and the memory tail metric (σ_m~~sigma m~~) both showed less than a doubling between short and long tubing. These modest differences in wall-effect memory metrics are not explained by the theory in Pagonis et al. (2017).~~While there are slight differences in these memory metrics, this is likely due to the influence of the analyzer. length does not seem The difference in length appears in the mixing time scales and the memory tail metric both showed less than a doubling. Becauseut bBecause the residence time and attenuation time metrics of the short FEP tubing (1.181.0 ± 0.09 s) was smaller than that of the analyzer (~ 4 s), we are not able to see the short tubing effects individually. This also indicates that to be seen by our analyzer, tubing memory must have a resolution of greater than 4 s. It follows that the ~ 1.5 s mixing time found when measuring short thick walled FEP is likely the "'best case scenario'" based on analyzer mixing, and any additional mixing time is due to tubing effects.~~

~~{paragraph on holding everything constant except ID, and then later holding ID constant and changing material}~~ The tubing ID affects the residence, lag, and location times, the surface area to air volume ratios, and the flow velocity past the surface of the tubing interior. Pagonis et al. (2017) predicts ~~threshold metrics~~the residence time of gas molecules on or in the tubing walls ~~-~~changes linearly with respect to tubing ID when ~~other tubing properties are the same~~the tubing material

Formatted
Formatted
Formatted
Formatted
Formatted
Formatted
Formatted
Formatted
Formatted
Formatted
Formatted
Formatted
Formatted
Formatted
Formatted
Formatted
Formatted
Formatted
Formatted
Formatted
Formatted
Formatted
Formatted
Formatted
Formatted
Formatted
Formatted
Formatted
Formatted
Formatted
Formatted
Formatted
Formatted
Formatted
Formatted
Formatted
Formatted
Formatted
Formatted
Formatted
Formatted
Formatted
Formatted
Field Code Changed
Formatted

does not change. In our experiments, ID increased by a factor of 1.5x between thick- and thin-walled FEP ($^1/_8$ in. or [illegible] FEP3 and 4 is exaggerated by the δ^{18}O location adjustment applied to the δD signal, but thin-walled FEP does have a slightly less steep slope and longer $t_{63\%}$ t63 intercept than the thick-walled tubing. rResidence time adjusted memory metrics also show a slight overall differences increase with ID increase between thick- and thin-walled tubing, with an average 1.9x larger memory metric for δD and 1.66x [illegible] consistently showed the slowest δD signal transitions of the tubings tested (Fig. 3, 4, S3, and S4 panels c and dTable S2). FromIn the location adjusted comparison in of the same material (FEP) with different lengths and IDs (Fig.ure 4, δ^{18}O location adjusted [illegible] the same approximate tubing length and $^3/_{16}$ in. (~4.76 mm) ch ID and length and those experiments showed a faster attenuation threshold time than FEP (Fig.ure 3). [illegible] tubing ID, material density, and partitioning depth will affect the residence time of chemical compounds on or in a [illegible]

In summary, we found that all tubing dimensions, including ID and length, had some effects on the threshold metrics (Fig. 4 and S4) after removing differences in residence times in signal propagation to the analyzer based on tubing inner volume and the temperature influence on molecular density. While these overall memory metric differences exist, they are small in the materials and dimensions tested, and the operational impact among commonly used ¼ in. (6.35 mm) OD tubing inlets is expected to be limited.

4.34 Relative attenuation time differences between δD and δ^{18}O

δδD signals have been demonstrated to take longer than δδ^{18}O signals to isotopically equilibrate with tubing materials than δ^{18}O due to isotope-dependent hydrogen- bonding interactions with the tubing walls (Sturm and Knohl, 2010; Griffis et al., 2010; Schmidt et al., 2010). This speed difference has been reported as a ratio of attenuation times between the slower δδD signal and the faster δδ^{18}O signals, and a large range of values ratios have been reported. Published results show 1.4 –3.5x Under air flow conditions of 12 L min^{-1}, Griffis et al. (2010) suggests a 3.5x greater attenuation time for δD signals than δ^{18}O signals in spectral analysis, depending on tubing air flow rates, and tubing type, and memory metric used (Schmidt et al., 2010; Griffis et al., 2010; Aemisegger et al., 2012; Zannoni et al., 2022). Schmidt et al.'s (2010) PFA experiments over a range of water vapor concentrations found a 1.6–3.3x greater $t_{95\%}$ time for δD signals than δ^{18}O. We found a 1.57x greater $t_{95\%}$ time value for δD signals than δ^{18}O under slow analyzer conditions and 1.49x greater $t_{95\%}$ value in fast analyzer tests, which is comparable to Schmidt et al. (2010). For ρ_S – $t_{63\%}$, we found a 0.71.1 –1.84x greater attenuation time for δD signals than δ^{18}O signals. The ρ_S metric is not particularly sensitive to the characteristic long δD memory tail. under slow analyzer conditionsFor ρ_m, δD values were 0.91.0 –1.7x longer than δ^{18}O values, which is a metric more sensitive to the characteristic long δD memory tail. These ranges are similar to the previously published results. Location ratios were very similar at 1.0 –1.1x.xxx greater for δD signals than δ^{18}O which is understandable because that indicates the time of rapid flushing of the analyzer cavity when the new source vapor reaches the analyzer. For $t_{63\%}$, this ratio ranges from 1.20 –4.91.2x greater, and for $t_{95\%}$ 1.0–2.74.2x. The threshold metrics are most similar to the

The relative equilibration speed differences in δD and δ^{18}O signals leads to a transient anomaly in D-excess signals (Figures 3,4, S1, and S22 panels e and f, and Figure 4 panels c and f)., as theIn the enriched-to-depleted transition, propagation of the depleted δD signal was delayed relative to the depleted δ^{18}O signal (as shown by the orangegray lines in Figures 3 2 and S1 panels b and d), creating a transient positive anomaly in D-excess before equilibrating with the new vapor source isotopic values. Since the shape of the time-varying D-excess anomaly is different from δD and δ^{18}O, and is not unidirectional, the time to equilibrium must be quantified differently. The time scale for tubing to equilibrate for D-excess was longer than both δ^{18}O and δD. On average it took approximately 33 seconds17.5 minutes for the transient anomaly to decay to within 3‰ of the ultimate equilibrium value after location adjustment. Smaller isotopic step changes and faster air flow rates will lead to shorter t3 threshold attenuation times.

Lag/location times were decreased by shortening the intake tubing and increasing flow through the analyzerlength and inner diameter (Figure 4). The lag time can be mathematically calculated as the residence time of air in the [redacted] effectively the same reverse sigmoidal shape after fitted location time adjustment, with varying amounts of spread. The slight differences in signal attenuation curve shapes could be due to small variations in tubing length, uncertainties in lag time corrections, and uncertainties errors in normalization and location adjustments between experiments, differences in tubing internal roughness, and analyzer noise, as well as differences in the mixing times indicating diffusion of the signal front. Previous studies approximated the attenuation response transfer function as an exponential curve (Sturm and Knohl, 2010; Aemisegger et al., 2012; Schmidt et al., 2010), where the signal front follows a perfect plug flow similar to the exponential decay response that would be expected for the residence time distribution function of a continuously stirred reactor (Toson et al., 2019)(cite)consistent with the mixing theory for a continuous stirred reactor (Toson et al., 2019). We found the exponential function was not a satisfactory fit to our experimental observations. A more appropriate mixing analogy could be the axially dispersed plug flow (ADPF) model (Huang and Seinfeld, 2019), as this better matches the reverse sigmoid curve we observe.. In the ADPF is model, there is a bulk flow that has a diffusive ""head"" that diverges forwards and backwards from the bulk flow, leading to the observed smoothing of the output signal of an input step-change. This effectively ""smears"" the observed isotopic signal. While the shape of this transfer function seems appropriate, the Huang and Seinfeld (2019) model does not consider gas-wall exchange effects. The transfer function model we introduce here fits the observations sufficiently well, but more work is needed to match the formulas with mixing theory.

Likewise, the impulse fitting method we used is more complicated than previously used (cite Jones)(Jones et al., 2017; Kahle et al., 2018). For the impulse response method portion of the data workup, we took inspiration from [redacted] modified impulse function fitting method. We believe these metrics are a signals of diffusion mixing and isotopic wall [redacted] potentially useful for correcting out memory effects in vaporwater vapor isotope measurements, as suggested by Massman and Ibrom (2008) and others (e.g. Aemisegger et al., 2012; Steen-Larsen et al., 2014). Similar corrections and have been

Formatted: Not Highlight
Formatted: Not Highlight
Formatted: Highlight
Formatted: Not Highlight
Formatted: Font: Times New Roman
Formatted: Indent: First line: 0"
Formatted: Font: Times New Roman, Not Highlight
Formatted: Font: Times New Roman
Formatted: Font: Times New Roman, Not Highlight
Formatted: Font: Times New Roman
Formatted: Font: Times New Roman, Not Highlight
Formatted: Font: Times New Roman
Formatted: Font: Times New Roman, Highlight
Formatted: Font: Times New Roman
Formatted: Font: Times New Roman, Highlight
Formatted: Font: Times New Roman
Formatted: Font: Times New Roman, Highlight
Formatted: Font: Times New Roman
Formatted: Font: Not Bold
Formatted: Not Highlight
Formatted: Not Highlight
Field Code Changed
Formatted: Not Highlight
Formatted: Highlight
Field Code Changed
Field Code Changed
Formatted: Not Highlight
Formatted: Not Highlight
Formatted: Not Highlight
Formatted: Not Highlight
Formatted: Font: Times New Roman, Not Highlight
Formatted: Font: Times New Roman, Not Highlight
Formatted: Font: Times New Roman, Not Highlight
Formatted: Font: Times New Roman, Not Highlight

achieved in the ice core and liquid water isotope analysis communities (e.g. Jones et al., 2017; Kahle et al., 2018; Vallet-Coulomb et al., 2021). We found more complicated transfer and impulse function models were necessary to fully capture the memory effects in the vapor inlet system compared to the mostly liquid inlet systems described before (e.g. Jones et al., 2017; Kahle et al., 2018; Vallet-Coulomb et al., 2021). This should provide a starting point for future work

5 Implications for measurements

Longer attenuation times smooth signal variability and mask high-frequency features. Therefore, the magnitude and speed of atmospheric signal variability as well as the analyzer and sample intake performance are important considerations when planning for ambient water vapor isotopic measurements. Analyzer signal attenuation times were found to be most sensitive to analyzer air flow rates and a mass flow meter, withWe found very small differences among tubing materials under the experimental conditions tested here. While different analyzer air flow rates are not presented in this study, it is known that analyzer flow rate strongly influences sample residence time in the optical cavity of these analyzers and the speed of signal transitions. The Aemisegger et al., (2012) findings thate analyzer flow rate and internal tubing have a larger effect on attenuation times were controlled more by analyzer residence times than PFA intake tubing in their experiments is supported by the results presented in this study.

We also suggest testing the effect of any in-line elements like mass flow meters, controllers, or filters on isotopic signal attenuation, especially if they are made from materials not tested in this study. The internal materials and geometry of the Omega mass flow meter are currently unknown but had a large effect on isotopic signal attenuation. Though Bev-A-Line XX was the only we did not find any materials in this studytesing that performed particularly poorly, prior research clearly identified Dekabon tubing as unsuitable (Sturm and Knohl, 2010; Griffis et al., 2010; Schmidt et al., 2010; Tremoy et al., 2011). We also suggest testing the effect of any in-line elements like flow meters, mass flow controllers, or filters on isotopic signal attenuation, especially if they are made from materials not tested in this study. Our experience found a mass flow meter that introduced a large memory effect (not presented here). These considerations should maximize D-excess data resolution.

5.1 Low atmospheric variability measurements

For stationary measurements with one intake and high air flow rates, tubing selection among commonly used materials is not as much of a concern as air advecting past the intake typically changes slowly compared to tubing attenuation time scales we quantify here. Conroy et al., (2016) for example, observed vapor on Manus Island, Papua New Guinea that changed by 22.3 ‰ in $\delta^{18}O$ and 154.8 ‰ in δD, with the largest change being ~25 ‰ δD over a duration of a few hours. The instant isotopic step change in our experiment (17.6 ‰ in $\delta^{18}O$ and 136 ‰ in δD) in our experiment is extreme compared to typical atmospheric variability at a stationary inlet. For stationary measurements, any of the tested tubing materials besides Bev-aA-Lline XX should be suitable and would not be expected to produce large transient D-excess artifacts due to memory differences between δD and $\delta^{18}O$.

Formatted: Font: 10 pt, Bold, Font color: Black, Kern at 16 pt

Formatted: Not Highlight

Formatted: Highlight

Formatted: Not Highlight

5.2 High atmospheric variability measurements

For measurements that need high temporal resolution of small atmospheric isotopic variability like flux gradient and eddy covariance setups or airborne observations, extra precautions should be taken. ~~This is also asserted by Aemisegger et al., (2012), who state that the analyzer flow rate and internal tubing have a larger effect on attenuation time than the PFA intake tubing in their experiments.~~ Griffis et al. (2010) used spectral analysis in their eddy covariance experiments to show that tube memory effects weren't a concern for $\delta^{18}O$ signals at tubing air flow rates of 12 L min^{-1} and analyzer air flow rates of 1.5 L min^{-1}. However, one can't extend that conclusion to slower air flow rates and analyzer residence times should be compared across analyzer types.

Aircraft campaigns are a special concern, as they observe not only at high temporal (and spatial) resolution, but ~~record~~ encounter large and rapid isotopic and humidity variability as well. Especially when conducting vertical profiles, isotopic compositions can vary by hundreds of per mil in δD. Salmon et al. (2019) found δD signal values ranging from -400 to -175 ‰ δD within an ~5 minute vertical profile descent between 1200 to 400 m above ground. Similarly, Sodemann et al. (2017) reported flight sections with >200 ‰ δD variations in under 5 minutes. While data was collected at 1 Hz, their reported data is a 15 s~~econd~~ average, which allows them a 975 m horizonal and 75 m vertical resolution (Sodemann et al., 2017). However, that best-case estimate is based on the data averaging interval and does not consider signal attenuation due to tubing isotopic memory or mixing in the optical cavity (Sodemann et al., 2017). Additionally, averaging over long time periods may not remove D-excess memory bias depending on patterns of increasing or decreasing delta values. The wetting and drying of the measurement system during flights with large changes in altitude, and therefore atmospheric specific humidity, may also increase isotopic attenuation times but were not quantified here.

In both eddy covariance and aircraft measurement situations, one might consider increasing air flow through the analyzer and intake tubing and shortening the length of tubing from an intake pickoff point to the analyzer in slow analyzer flow setups as has been suggested in previous studies (e.g. Griffis et al., 2010). While high air flow rates can easily be achieved in the air intake main lines in both high-frequency measurement situations, the air flow rate through the analyzer is typically limited by the analyzer design and control software. If ~~When~~ tubing or in-line elements like mass flow controllers ~~walls~~ affect the speed at which the isotopes are transmitted from the intake to the optical cavity, signals are effectively low-pass filtered (Zannoni et al., 2022). Our experiments show shorter memory effects for shorter tubing compared to longer tubing. Therefore, it is also important to minimize the length of tubing from the intake pickoff point to the analyzer ~~(as increased lengths increase lag/location time)~~ to reduce the residence time of air in the low-flow portion of the system. These considerations should also maximize D-excess data resolution.

Formatted: Not Highlight

Formatted: Not Highlight

Field Code Changed

Formatted: Not Highlight

5.3 Liquid water measurements

Liquid water isotope analysis is also plagued by memory effects when samples are converted to the vapor phase for spectral isotopic analysis, especially in applications measuring samples with large isotopic differences in the same batch. Common protocols recommend multiple replicate injections and discarding the first few to remove carryover

from the previous sample (IAEA, 2009; Penna et al., 2012; Coplen and Wassenaar, 2015). In both OA-ICOS and cavity ring-down spectroscopy, Penna et al. (2012) found that when measuring samples with large isotopic differences, up to eight out of eighteen injections had to be ignored to limit memory effects. When analyzing highly ~~-~~depleted Antarctic samples ranging from −231.7 ‰ to −421.1 ‰ for δD, memory effects of up to 14 ‰ were found in the first injection compared to the "true" value. Liquid water analysis is one example of a case where air flow rates and temperatures of transfer lines are fixed by the instrument design. Material properties inside the analyzer are important, but this study finds little difference between commonly used material types. Waiting for equilibrium in the optical cavity may minimize the memory effect, but a time-efficient method to increase sample throughput is to mathematically correct for these repeatable effects rather than attempting to minimize them (~~–~~e.g. de Graaf et al., 2020; Vallet-Coulomb et al., 2021; Hachgenei et al., 2022). ~~- O(~~ e.g. Vallet-Coulomb et al., 2021; Hachgenei et al., 2022~~).~~ Or, ~~-Or~~ in the case of de Graaf et al., (2020), one can ~~to~~ measure small vapor samples on a background of humid air to reduce memory effects. Work is also being done in the ice core community to correct out signal mixing ~~using curve fitting models~~based on transfer function fitting methods (e.g Jones et al., 2017; Kahle et al., 2018) ~~as discussed in the methods~~. These memory correction approaches may provide examples of methods to reconstruct input signal variability from smoothed continuous vapor isotope measurements as well.

6 Conclusions

We tested the water isotopic exchange properties of PFA, FEP, PTFE, HDPE, ~~and~~ copper, and Bev-A-Line XX. The commonly ~~-~~used materials tested here perform similarly. It does not seem necessary to s~~S~~tandardize~~zing~~ materials used to measure stable water vapor isotopologues ~~does not seem necessary~~ to make accurate and comparable measurements in most situations, when using analyzers with similar residence times, ~~as the commonly used materials tested here perform similarly~~. We ~~cannot~~ recommend Bev-A-Line XX for use in water vapor applications due to extremely long attenuation times. ~~Temperature did not seem to affect memory effects, and~~ Warmer temperatures did shorten the residence time, lag, and location metrics of the impulse function and ~~t63%~~ $t_{63\%}$ ~~-~~threshold times across all long tubing experiments ~~but was not always consistent. The influence of the humidity of the purge air was not fully explored in this study~~. ~~While differences may be found among higher quality~~ ~~were and longer lengths were~~ predicted to increase ~~-~~memory metrics proportionally based on gas-wall partitioning theory (Pagonis et al., 2017), and we found that tubing ID and length had some effects on the threshold metrics after removing differences in residence times. The experiments here showed overall memory metric differences do exist, but that they are small in the materials and dimensions tested. In experimental settings, operational impact among commonly used ¼ in. (6.35 mm) OD tubing is expected to be ~~in the experiments here. Low air flow rates and temperatures were found to increase memory metrics proportionally based on gas-wall partitioning theory (Pagonis et al., 2017)~~.

Researchers must understand the limitations of the air flow conditions and wall effects of their instrumental and intake setups to limit signal memory effects, especially if low air flow rates are a constraint or if there are large isotopic variations over short periods of time. Our experience and results from other published studies indicate that maximizing air flow rates through the analyzer is the most effective way to minimize memory effects when accurate high-frequency D-excess measurements are desired.

Formatted: Not Highlight

Field Code Changed

Formatted: Not Highlight

Formatted: Highlight

Formatted: Indent: First line: 0.25"

Formatted: Not Highlight

Code/Data Availability

All figure data and scripts, as well as an example workup code, are available at https://doi.org/10.4231~~/~~/T6J3~~H7ZJ-H6496J45~~ (Meyer and Welp, 2023).

Author Contributions

ALM and LRW designed the experiments and ~~, while ALM~~ conducted them. ALM adapted code ~~(~~from LRW ~~)~~ and added to it for this project, as well as analyzed data. ALM wrote the manuscript draft~~, with the section on exchange sites by LRW~~. ALM and LRW edited the document.

Competing Interests

The authors declare that they have no conflict of interest.

Acknowledgements

We thank Matthew Binkley (MS Materials Engineering) for valuable discussion of material properties.

Financial Support

AM was supported by a Purdue Doctoral Fellowship and the National Science Foundation Graduate Research Fellowship Program under Grant No. (DGE-1333468). Any opinions, findings, and conclusions or recommendations expressed in this material are those of the authors and do not necessarily reflect the views of the National Science Foundation.

Review Statement

~~This paper was edited by~~We thank the editor Thomas Röckmann and ~~reviewed by~~ three anonymous referees, as well as community commenter Jonathan Keinan~~. We thank all five~~ for their time, suggestions for improvement, and patience~~effort~~.

Field Code Changed

Formatted: Not Highlight

Formatted: Highlight

Formatted: Font: (Default) Times New Roman, 10 pt, Font color: Auto, Pattern: Clear

References

Aemisegger, F., Sturm, P., Graf, P., Sodemann, H., Pfahl, S., Knohl, A., and Wernli, H.: Measuring variations of $\delta^{18}O$ and $\delta^{2}H$ in atmospheric water vapour using two commercial laser-based spectrometers: an instrument characterisation study, Atmos. Meas. Tech., 5, 1491–1511, https://doi.org/10.5194/amt-5-1491-2012, 2012.

Ardia, D., Mullen, K., Peterson, B., Ulrich, J., and Boudt, K.: DEoptim: Global Optimization by Differential Evolution Version 2.2-8, CRAN [code], https://cran.r-project.org/package=DEoptim, 2022.

Chemours: An introduction to Chemours™ fluoropolymers, C–11311., The Chemours Company, FC, LLC, 2018. https://www.chemours.com/en/-/media/files/teflon/intro-to-fluoropolymers.pdf?rev=a43531c7fc5c406d86ced4425f2330b4, last access: 14 July 2022.

Conroy, J. L., Noone, D., Cobb, K. M., Moerman, J. W., and Konecky, B. L.: Paired stable isotopologues in precipitation and vapor: A case study of the amount effect within western tropical Pacific storms, Journal of Geophysical Research: Atmospheres, 121, 3290–3303, https://doi.org/10.1002/2015JD023844, 2016.

Coplen, T. B. and Wassenaar, L. I.: LIMS for Lasers 2015 for achieving long-term accuracy and precision of $\delta^{2}H$, $\delta^{17}O$, and $\delta^{18}O$ of waters using laser absorption spectrometry, Rapid Communications in Mass Spectrometry, 29, 2122–2130, https://doi.org/10.1002/rcm.7372, 2015.

Galewsky, J., Steen-Larsen, H. C., Field, R. D., Worden, J., Risi, C., and Schneider, M.: Stable isotopes in atmospheric water vapor and applications to the hydrologic cycle, Rev. Geophys., 54, 809–865, https://doi.org/10.1002/2015RG000512, 2016.

de Graaf, S., Vonhof, H. B., Weissbach, T., Wassenburg, J. A., Levy, E. J., Kluge, T., and Haug, G. H.: A comparison of isotope ratio mass spectrometry and cavity ring-down spectroscopy techniques for isotope analysis of fluid inclusion water, Rapid Communications in Mass Spectrometry, 34, e8837, https://doi.org/10.1002/rcm.8837, 2020.

Griffis, T. J., Sargent, S. D., Lee, X., Baker, J. M., Greene, J., Erickson, M., Zhang, X., Billmark, K., Schultz, N., Xiao, W., and Hu, N.: Determining the oxygen isotope composition of evapotranspiration using eddy covariance, Boundary-Layer Meteorol, 137, 307–326, https://doi.org/10.1007/s10546-010-9529-5, 2010.

Griffith, D. W. T., Jamie, I., Esler, M., Wilson, S. R., Parkes, S. D., Waring, C., and Bryant, G. W.: Real-time field measurements of stable isotopes in water and CO_2 by Fourier transform infrared spectrometry, Isotopes in Environmental and Health Studies, 42, 9–20, https://doi.org/10.1080/10256010500503098, 2006.

Guerrier, S., Balamuta, J., Bakalli, G., Molinari, R., Lee, J., Radi, A., Xu, H., Zhang, Y., and Claussen, N.: avar: Allan Variance Version 0.1.1, CRAN [code], https://CRAN.R-project.org/package=avar, 2020.

Gupta, P., Noone, D., Galewsky, J., Sweeney, C., and Vaughn, B. H.: Demonstration of high-precision continuous measurements of water vapor isotopologues in laboratory and remote field deployments using wavelength-scanned cavity ring-down spectroscopy (WS-CRDS) technology, Rapid Communications in Mass Spectrometry, 23, 2534–2542, https://doi.org/10.1002/rcm.4100, 2009.

Huang, Y. and Seinfeld, J. H.: A note on flow behavior in axially-dispersed plug flow reactors with step input of tracer, Atmospheric Environment: X, 1, 100006, https://doi.org/10.1016/j.aeaoa.2019.100006, 2019.

IAEA: Laser spectroscopic analysis of liquid water samples for stable hydrogen and oxygen isotopes, International Atomic Energy Agency, Vienna, Germany, 2009.

Jones, T. R., White, J. W. C., Steig, E. J., Vaughn, B. H., Morris, V., Gkinis, V., Markle, B. R., and Schoenemann, S. W.: Improved methodologies for continuous-flow analysis of stable water isotopes in ice cores, Atmospheric Measurement Techniques, 10, 617–632, https://doi.org/10.5194/amt-10-617-2017, 2017.

Kahle, E. C., Holme, C., Jones, T. R., Gkinis, V., and Steig, E. J.: A Generalized Approach to Estimating Diffusion Length of Stable Water Isotopes From Ice-Core Data, Journal of Geophysical Research: Earth Surface, 123, 2377–2391, https://doi.org/10.1029/2018JF004764, 2018.

Kerstel, E. R. T., Iannone, R. Q., Chenevier, M., Kassi, S., Jost, H.-J., and Romanini, D.: A water isotope (^{2}H, ^{17}O, and ^{18}O) spectrometer based on optical feedback cavity-enhanced absorption for in situ airborne applications, Appl. Phys. B, 85, 397–406, https://doi.org/10.1007/s00340-006-2356-1, 2006.

Lee, X., Sargent, S., Smith, R., and Tanner, B.: In situ measurement of the water vapor ^{18}O/^{16}O isotope ratio for atmospheric and ecological applications, J. Atmos. Oceanic Technol., 22, 555–565, https://doi.org/10.1175/JTECH1719.1, 2005.

Luo, H., Pingintha-Durden, N., and Smith, D.: NEON sensor command, control and configuration (C3) document: eddy covariance storage exchange (NEON.DOC.000465) Version F, NEON (National Ecological Observatory Network), 71, 2019.

Managave, S., Jani, R., Narayana Rao, T., Sunilkumar, K., Satheeshkumar, S., and Ramesh, R.: Intra-event isotope and raindrop size data of tropical rain reveal effects concealed by event averaged data, Climate Dynamics, 47, 981–987, https://doi.org/10.1007/s00382-015-2884-7, 2016.

Massman, W. J. and Ibrom, A.: Attenuation of concentration fluctuations of water vapor and other trace gases in turbulent tube flow, Atmospheric Chemistry and Physics, 8, 6245–6259, https://doi.org/10.5194/acp-8-6245-2008, 2008.

Meyer, A. and Welp, L. R.: Water vapor stable isotope memory effects of common tubing materials, https://doi.org/10.4231/T6J3-H649, 2023.

Muggeo, V. M. R.: segmented: Regression models with break-points / change-points (with possibly random effects) estimation Version 1.6-0, CRAN [code], https://CRAN.R-project.org/package=segmented, 2022.

Pagonis, D., Krechmer, J. E., de Gouw, J., Jimenez, J. L., and Ziemann, P. J.: Effects of gas–wall partitioning in Teflon tubing and instrumentation on time-resolved measurements of gas-phase organic compounds, Atmospheric Measurement Techniques, 10, 4687–4696, https://doi.org/10.5194/amt-10-4687-2017, 2017.

Penna, D., Stenni, B., Šanda, M., Wrede, S., Bogaard, T. A., Michelini, M., Fischer, B. M. C., Gobbi, A., Mantese, N., Zuecco, G., Borga, M., Bonazza, M., Sobotková, M., Čejková, B., and Wassenaar, L. I.: Technical Note: Evaluation of between-sample memory effects in the analysis of δ^{2}H and δ^{18}O of water samples measured by laser spectroscopes, Hydrology and Earth System Sciences, 16, 3925–3933, https://doi.org/10.5194/hess-16-3925-2012, 2012.

Electrical properties of plastic materials: https://www.professionalplastics.com/professionalplastics/ElectricalPropertiesofPlastics.pdf, last access: 17 December 2021.

R Core Team: R: A Language and Environment for Statistical Computing, http://www.R-project.org/, 2023.

Salmon, O. E., Welp, L. R., Baldwin, M. E., Hajny, K. D., Stirm, B. H., and Shepson, P. B.: Vertical profile observations of water vapor deuterium excess in the lower troposphere, Atmospheric Chemistry and Physics, 19, 11525–11543, https://doi.org/10.5194/acp-19-11525-2019, 2019.

Schmidt, M., Maseyk, K., Lett, C., Biron, P., Richard, P., Bariac, T., and Seibt, U.: Concentration effects on laser-based δ^{18}O and δ^{2}H measurements and implications for the calibration of vapour measurements with liquid standards, Rapid Commun. Mass Spectrom., 24, 3553–3561, https://doi.org/10.1002/rcm.4813, 2010.

Sodemann, H., Aemisegger, F., Pfahl, S., Bitter, M., Corsmeier, U., Feuerle, T., Graf, P., Hankers, R., Hsiao, G., Schulz, H., Wieser, A., and Wernli, H.: The stable isotopic composition of water vapour above Corsica during the HyMeX SOP1 campaign: insight into vertical mixing processes from lower-tropospheric survey flights, Atmos. Chem. Phys., 17, 6125–6151, https://doi.org/10.5194/acp-17-6125-2017, 2017.

Steen-Larsen, H. C., Sveinbjörnsdottir, A. E., Peters, A. J., Masson-Delmotte, V., Guishard, M. P., Hsiao, G., Jouzel, J., Noone, D., Warren, J. K., and White, J. W. C.: Climatic controls on water vapor deuterium excess in the marine boundary layer of the North Atlantic based on 500 days of in situ, continuous measurements, Atmospheric Chemistry and Physics, 14, 7741–7756, https://doi.org/10.5194/acp-14-7741-2014, 2014.

Sturm, P. and Knohl, A.: Water vapor δ^2H and $\delta^{18}O$ measurements using off-axis integrated cavity output spectroscopy, Atmos. Meas. Tech., 3, 67–77, https://doi.org/10.5194/amt-3-67-2010, 2010.

Toson, P., Doshi, P., and Jajcevic, D.: Explicit residence time distribution of a generalised cascade of continuous stirred tank reactors for a description of short recirculation time (bypassing), Processes, 7, 615, https://doi.org/10.3390/pr7090615, 2019.

Tremoy, G., Vimeux, F., Cattani, O., Mayaki, S., Souley, I., and Favreau, G.: Measurements of water vapor isotope ratios with wavelength-scanned cavity ring-down spectroscopy technology: new insights and important caveats for deuterium excess measurements in tropical areas in comparison with isotope-ratio mass spectrometry, Rapid Communications in Mass Spectrometry, 25, 3469–3480, https://doi.org/10.1002/rcm.5252, 2011.

Vallet-Coulomb, C., Couapel, M., and Sonzogni, C.: Improving memory effect correction to achieve high-precision analysis of $\delta^{17}O$, $\delta^{18}O$, δ^2H, ^{17}O-excess and d-excess in water using cavity ring-down laser spectroscopy, Rapid Communications in Mass Spectrometry, 35, e9108, https://doi.org/10.1002/rcm.9108, 2021.

Webster, C. R. and Heymsfield, A. J.: Water isotope ratios D/H, $^{18}O/^{16}O$, $^{17}O/^{16}O$ in and out of clouds map dehydration pathways, Science, 302, 1742–1745, https://doi.org/10.1126/science.1089496, 2003.

Zannoni, D., Steen-Larsen, H. C., Peters, A. J., Wahl, S., Sodemann, H., and Sveinbjörnsdóttir, A. E.: Non-equilibrium fractionation factors for D/H and $^{18}O/^{16}O$ during oceanic evaporation in the north-west Atlantic region, Journal of Geophysical Research: Atmospheres, 127, e2022JD037076, https://doi.org/10.1029/2022JD037076, 2022.